Circulation: Arrhythmia and Electrophysiology

ORIGINAL ARTICLE

Enhanced Depolarization Drive in Failing Rabbit Ventricular Myocytes

Calcium-Dependent and β-Adrenergic Effects on Late Sodium, L-Type Calcium, and Sodium-Calcium Exchange Currents

Bence Hegyi, MD, PhD
Stefano Morotti, PhD
Caroline Liu
Kenneth S. Ginsburg, PhD
Julie Bossuyt, DVM, PhD
Luiz Belardinelli, MD
Leighton T. Izu, PhD
Ye Chen-Izu, PhD
Tamás Bányász, MD, PhD
Eleonora Grandi, PhD
Donald M. Bers, PhD

BACKGROUND: Heart failure (HF) is characterized by electrophysiological remodeling resulting in increased risk of cardiac arrhythmias. Previous reports suggest that elevated inward ionic currents in HF promote action potential (AP) prolongation, increased short-term variability of AP repolarization, and delayed afterdepolarizations. However, the underlying changes in late Na^+ current (I_{NaL}), L-type Ca^{2+} current, and NCX (Na^+/Ca^{2+} exchanger) current are often measured in nonphysiological conditions (square-pulse voltage clamp, slow pacing rates, exogenous Ca^{2+} buffers).

METHODS: We measured the major inward currents and their Ca^{2+}- and β-adrenergic dependence under physiological AP clamp in rabbit ventricular myocytes in chronic pressure/volume overload–induced HF (versus age-matched control).

RESULTS: AP duration and short-term variability of AP repolarization were increased in HF, and importantly, inhibition of I_{NaL} decreased both parameters to the control level. I_{NaL} was slightly increased in HF versus control even when intracellular Ca^{2+} was strongly buffered. But under physiological AP clamp with normal Ca^{2+} cycling, I_{NaL} was markedly upregulated in HF versus control (dependent largely on CaMKII [Ca^{2+}/calmodulin-dependent protein kinase II] activity). β-Adrenergic stimulation (often elevated in HF) further enhanced I_{NaL}. L-type Ca^{2+} current was decreased in HF when Ca^{2+} was buffered, but CaMKII-mediated Ca^{2+}-dependent facilitation upregulated physiological L-type Ca^{2+} current to the control level. Furthermore, L-type Ca^{2+} current response to β-adrenergic stimulation was significantly attenuated in HF. Inward NCX current was upregulated at phase 3 of AP in HF when assessed by combining experimental data and computational modeling.

CONCLUSIONS: Our results suggest that CaMKII-dependent upregulation of I_{NaL} in HF significantly contributes to AP prolongation and increased short-term variability of AP repolarization, which may lead to increased arrhythmia propensity, and is further exacerbated by adrenergic stress.

VISUAL OVERVIEW: A visual overview is available for this article.

Key Words: action potential ■ buffers ■ electrophysiology ■ heart failure ■ rabbits

https://www.ahajournals.org/journal/circep

WHAT IS KNOWN?

- Significant ion channel remodeling occurs in heart failure (HF), which results in prolongation of the cardiac action potential (and QT interval in ECG) and increases the risk of arrhythmias.
- Enhanced late Na^+ current and upregulation of NCX (Na^+/Ca^{2+} exchanger) have been reported in HF.

WHAT THE STUDY ADDS?

- CaMKII (Ca^{2+}/calmodulin-dependent protein kinase II)-dependent and β-adrenergic upregulation of late Na^+ current in HF enhances the net depolarization drive and significantly contributes to arrhythmogenic action potential alterations in HF.
- L-type Ca^{2+} current exhibits CaMKII-dependent facilitation but β-adrenergic hyporesponsiveness in HF.

Heart failure (HF) is characterized by increased risk for cardiac arrhythmias. Arrhythmogenic alterations in the ventricular action potential (AP), including early and delayed afterdepolarizations,[1–4] AP duration (APD) prolongation,[5,6] and increased beat-to-beat variability of APD,[6–8] have been extensively studied in failing ventricular cardiomyocytes. Alterations in membrane potential stability have been associated with extensive ionic remodeling, including enhanced NCX (Na^+/Ca^{2+} exchanger) current (I_{NCX}),[9,10] increased late Na^+ current (I_{NaL}),[11,12] and reduced repolarization reserve.[13,14] In line with the electrophysiology results, the protein expression level of NCX was also found to be increased in HF,[9] whereas that of several K^+ channels was decreased.[15] But in the case of Na^+ channels, both the protein level and peak current density were decreased,[12,16] suggesting that the increased I_{NaL} in HF results from altered regulation and gating. Accordingly, CaMKII (Ca^{2+}/calmodulin-dependent protein kinase II) was found to be centrally involved in I_{NaL} upregulation in HF.[17–19]

However, I_{NaL} in previous HF studies was typically measured in nonphysiological conditions (square-pulse voltage clamp, slow stimulation rates, strong buffering of intracellular Ca^{2+} concentration ($[Ca^{2+}]_i$), and room temperature), which might have masked some important aspects of I_{NaL} regulation. Indeed, I_{NaL} was found to be larger in AP-clamped healthy guinea pig and rabbit myocytes than the tiny I_{NaL} found in conventional voltage-clamp studies.[20,21] βAR (β-adrenergic receptor) stimulation can further enhance I_{NaL} (via both CaMKII-dependent and independent mechanisms[19,21,22]), and increased sympathetic activity is commonly observed in HF. Consequently, enhanced I_{NaL} in HF may play a critical role in APD prolongation leading to cardiac arrhythmias and Na^+ overload.[23] Accordingly, inhibition of either I_{NaL} or CaMKII was found to exert beneficial effects in HF.[18,24] Unlike upregulated I_{NCX} and I_{NaL}, L-type Ca^{2+} current (I_{CaL}) was found to be unchanged or slightly decreased in previous studies in HF.[4,25,26] However, because βAR signaling, Ca^{2+}, and CaMKII all regulate I_{CaL},[27–29] prior voltage-clamp studies could easily misestimate changes in physiological I_{CaL} or I_{NaL} that occur during the AP in HF.

The present study measures APD, I_{NaL}, I_{CaL}, and I_{NCX} in HF versus control rabbit hearts during physiological APs, with or without βAR activation, and also assesses the involvement of CaMKII. We performed AP-clamp recordings with physiological ionic composition, pacing rate, $[Ca^{2+}]_i$, and temperature. We hypothesized that Ca^{2+} transients and increased CaMKII activity under these conditions significantly enhance inward currents in HF leading to arrhythmogenic alterations in AP morphology. We used a previously well-characterized chronic nonischemic HF rabbit model (combined volume and pressure overload), which is also arrhythmogenic.[4,9,14,30] APs and major inward ionic currents were measured under current and AP clamp, respectively, in ventricular myocytes using specific blockers of I_{NaL} (GS-967) and I_{CaL} (nifedipine). Because under physiological conditions, our nifedipine-sensitive current (I_{Nife}) includes both I_{CaL} and some inward I_{NCX} (because nifedipine inhibits Ca^{2+} transients that modulate I_{NCX}), we included computational modeling to better clarify the distinct profiles of I_{CaL} and I_{NCX} under AP clamp. Modulation of I_{CaL} and I_{NaL} by Ca^{2+}, CaMKII, and βAR stimulation (ie, pathophysiological settings characteristic of HF) was also investigated to assess the regulatory changes in the net depolarizing drive during the plateau and repolarization phases of the AP.

METHODS

The data that support the findings of this study are available from the corresponding author on reasonable request. All animal handling and laboratory procedures were in accordance with the approved protocols of the local Institutional Animal Care and Use Committee confirming to the Guide for the Care and Use of Laboratory Animals published by the US National Institutes of Health (eighth edition, 2011).

Arrhythmogenic Rabbit Nonischemic HF Model

HF was induced in New Zealand white rabbits (all male, 2.5–3 kg, and 3–4 months old) by aortic insufficiency and 4 weeks later by aortic constriction as described previously.[9] Data here were obtained from 12 HF rabbits and 8 age-matched control rabbits. HF progression was monitored periodically by echocardiography, and myocytes were isolated when left ventricular end-systolic dimension exceeded 1.4 cm (at ≈2.5 years of age). HF animals versus control hearts were near twice the heart weight/body weight (5.27±0.61 versus 2.67±0.10 g/kg; $P<0.01$), exhibited ≈40% larger

left ventricular end-diastolic diameter (2.31±0.10 versus 1.61±0.08 cm; P<0.001), ≈50% larger left ventricular end-systolic diameter (1.63±0.08 versus 1.08±0.05 cm; P<0.001), evidence of pulmonary congestion (lung weight, 19.13±2.29 versus 14.11±0.40 g; P<0.05), and abdominal ascites fluid accumulation, all similar to our prior studies on this rabbit model.[4,9,14] Enzymatic isolation of cardiomyocytes from the midmyocardial region of the left ventricular free wall was performed as described previously.[14]

Electrophysiology

Isolated cells were transferred to a temperature-controlled plexiglass chamber (Cell Microsystems) and continuously superfused with a modified, bicarbonate-containing Tyrode's solution containing (in mmol/L) NaCl 124, $NaHCO_3$ 25, KCl 4, $CaCl_2$ 1.2, $MgCl_2$ 1, HEPES 10, and Glucose 10, with pH 7.4. APs and underlying ionic currents were recorded in whole-cell configuration of patch-clamp technique. Electrodes were fabricated from borosilicate glass (World Precision Instruments) with tip resistances of 2 to 2.5 MΩ when filled with internal solution containing (in mmol/L) K-aspartate 110, KCl 25, NaCl 5, Mg-ATP 3, HEPES 10, cAMP 0.002, phosphocreatine-K_2 10, and EGTA 0.01, with pH=7.2. This composition preserved physiological myocyte Ca^{2+} transient and contraction.[20,31,32] Electrodes were connected to the input of an Axopatch 200B amplifier (Axon Instruments), with outputs digitized at 50 kHz using Digidata 1440A A/D card (Molecular Devices) under software control (pClamp 10). Series resistance (on cell) was typically 3 to 5 MΩ and was compensated by 85%. Experiments were discarded when the series resistance was high or increased substantially (>10%) during experiments. Reported AP voltages are already corrected to the liquid junction potentials. All experiments were conducted at 37±0.1 C.

APs were recorded in current-clamp experiments where cells were stimulated with depolarizing pulses (1.5× the threshold amplitude, 2 ms duration) delivered via patch pipette at pacing frequencies from 1 to 5 Hz. After reaching steady state (3 minutes at each frequency), 50 consecutive APs were recorded to measure average behavior. Then pacing was returned to 1 Hz, and the selective I_{NaL} inhibitor GS-967 (1 μmol/L) was added to perfusate. When GS-967 effects stabilized (typically within 3 minutes), AP recordings at different pacing frequencies were repeated. APD at 95% of repolarization (APD_{95}) was determined. Series of 50 consecutive APs were analyzed to estimate short-term variability of APD_{95} (STV) according to the following formula: $STV=\Sigma(|APD_{n+1}-APD_n|)/[(n_{beats}-1)\times\sqrt{2}]$, where APD_n and APD_{n+1} indicate the durations of the n^{th} and $(n+1)^{th}$ APs, and n_{beats} denotes the total number of consecutive beats analyzed.[33] Changes in STV are presented as Poincaré plots of 50 consecutive APD_{95}.

AP-clamp experiments were conducted as described previously.[14,34,35] Briefly, the basic steps are as follows: (1) record the cell's steady-state AP under I-clamp (self AP clamp) or choose a previously recorded typical AP (canonical AP clamp). (2) Apply this AP onto the cell as voltage command under V-clamp at a given pacing frequency. The net current output (reference current) should reach steady state and be stable over time. (3) Isolate the current of interest by using its specific blocker to remove it from the net current output (compensation current). (4) The current of interest is obtained by subtraction: drug-sensitive current=reference current–compensation current. (5) Next, isolate the second current of interest by applying the second channel blocker; when it reaches steady state, another compensation current is recorded, and the second current of interest can be determined again by subtraction. Figure I in the Data Supplement shows a representative example. Under AP clamp, all ionic currents were recorded as difference currents after each specific blocker had reached its steady-state effect (≈3 minutes of perfusion). Sixty consecutive traces were recorded (to evaluate the stability) and averaged in each case before applying a drug (reference current) and 3 minutes after drug application (compensation current). GS-967 of 1 μmol/L and nifedipine of 10 μmol/L were used to measure I_{NaL} and I_{CaL} (including some I_{NCX}), respectively. As validated previously,[21] the GS-967–sensitive current recorded in our conditions is an excellent selective measure of I_{NaL}. Experiments were performed both when Ca^{2+} cycling was preserved (Physiol) and when $[Ca^{2+}]_i$ was buffered below the diastolic level using 10 mmol/L BAPTA [1,2-bis(2-aminophenoxy) ethane-N,N,N′,N′-tetraacetic acid] in the internal solution ($BAPTA_i$) to assess $[Ca^{2+}]_i$ sensitivity of these currents under AP clamp. To test the effect of CaMKII, cells were pretreated for 2 hours before experiment with the specific CaMKII inhibitor, AIP (autocamtide-2–related inhibitory peptide; cell-permeable myristoylated form, 1 μmol/L). Both the perfusion and pipette solutions were also supplemented with AIP. In experiments examining the effect of βAR stimulation, isoproterenol (ISO; 3–300 nmol/L) was applied on AP-clamped cells. After ISO reached a steady-state effect (≈2 minutes), blockers were added sequentially to the perfusion solution to measure I_{NaL} and I_{CaL}. All AP-clamp experiments were performed in Tyrode's solution supplemented with selective inhibitors of K^+ and Cl^- currents (5 mmol/L 4-aminopyridine for I_{to}, 1 μmol/L E-4031 for I_{Kr}, 1 μmol/L HMR-1556 for I_{Ks}, 300 μmol/L $BaCl_2$ for I_{K1}, 100 nmol/L apamin for I_{KCa}, and 30 μmol/L CaCCinh-A01 for I_{ClCa}). Experiments were excluded from analysis if significant rundown of I_{CaL} was observed (in periodic tests) or if membrane current did not reach steady state.

Conventional square-pulse voltage-clamp experiments to measure the biophysical parameters of I_{CaL} were performed using pipette solution containing 5 mmol/L EGTA and 2.1 mmol/L $CaCl_2$ (free $[Ca^{2+}]_i$=100 nmol/L using the MaxChelator software) and in the presence of selective K^+ and Cl^- channel inhibitors in the bath (as above), and Na^+ was replaced by Li^+ to inhibit NCX. I_{CaL} was measured using 500-ms-long voltage steps from holding potential of –80 mV to test potentials (between –40 and +20 mV) every 5 s (0.2 Hz stimulation) with a 50-ms prestep to –40 mV to inactivate Na^+ channels. To investigate Ca^{2+}/CaMKII dependence of I_{CaL}, a 100-ms-long depolarization pulse to 0 mV were used in every 0.5 s (2 Hz stimulation).

Ion currents were normalized to cell capacitance, determined in each cell using short (10 ms), hyperpolarizing pulses from –10 to –20 mV. Cell capacitance was 144.4±1.2 pF in age-matched controls (118 cells per 8 animals) versus 194.1±3.3 pF in HF (158 cells per 12 animals) using 2-sample Student t test; P<0.001.

Chemicals and reagents were purchased from Sigma-Aldrich, if not specified otherwise. E-4031 and HMR-1556 were from Tocris Bioscience. GS-967 was from Gilead.

Computational Modeling and Simulation

In silico experiments were performed using our recently updated rabbit ventricular myocyte model[36] that integrates detailed descriptions of membrane electrophysiology, Ca^{2+} and Na^+ handling,[37] PKA (protein kinase A) and CaMKII signaling pathways,[38] and myofilament contraction.[39] This model describes changes in CaMKII activity during each heartbeat, resulting in dynamic functional modulation of CaMKII phosphorylation targets (L-type Ca^{2+} channels, ryanodine receptors, and phospholamban). These effects are enhanced in HF, where CaMKII expression and activation is increased (and as in prior work, we elevated CaMKII content to 6-fold).[38] We updated our model to account for HF-induced remodeling, based on our new data here and our previous HF model (including 2-fold increase in NCX maximal transport rate and altered sarcoplasmic reticulum [SR] Ca^{2+} release and reuptake).[40] Based on our novel I_{CaL} observations here, we shifted steady-state activation (5 mV negative) but left steady-state inactivation unchanged in HF. We also reduced I_{CaL} maximal conductance (G_{CaL}) by 20% in HF, resulting in the unaltered peak I_{CaL} that we observed in control versus HF myocytes (Table I in the Data Supplement; Figure II in the Data Supplement).

We used our updated cellular models to simulate AP-clamp experiments at 2 Hz pacing in control and HF myocytes with physiological Ca^{2+} handling (Figure III in the Data Supplement; exhibiting reduced Ca^{2+} transients in HF) or with CaMKII inhibition (simulated by clamping fractional phosphorylation of CaMKII targets to the levels predicted without pacing). We applied the same AP trace used in wet AP-clamp experiments as the voltage command. All simulations were performed in MATLAB (The MathWorks, Natick, MA) using the stiff ordinary differential equation solver ode15s. Model code is available for download at https://somapp.ucdmc.ucdavis.edu/Pharmacology/bers/ or http://elegrandi.wixsite.com/grandilab/downloads.

Statistical Analysis

Data are presented as mean±SEM. The number of cells in each experimental group was reported as n=number of cells/number of animals. Statistical significance of differences was tested by paired Student *t* test or ANOVA with Bonferroni post-test as appropriate using Origin2016 software. Differences were deemed significant if P was <0.05.

RESULTS

Frequency-Dependent Changes in AP Shape and Effect of I_{NaL} Inhibition in HF

Figure 1 shows representative APs and group analysis in HF and age-matched control myocytes before and after treatment with the selective I_{NaL} inhibitor GS-967 (1 μmol/L). Baseline APD_{95} was longer in HF versus control at 1 Hz pacing (269.5±17.5 versus 199.2±7.7 ms; P<0.001; Figure 1A and 1B). GS-967 decreased APD_{95} in HF by 22% (to 211.6±6.8 ms; not significant) and also decreased APD_{95} in control but by only 13% (to 174.2±5.9 ms; P<0.001). At faster pacing rates, APD_{95} converged for HF and control and similarly for the +GS-967 treatment curves (Figure 1B). Resting membrane potential was slightly depolarized (by ≈4 mV; Figure 1C) in HF consistent with reduced I_{K1} in HF.[4,5,14] AP amplitude was significantly lower (by 8–10 mV) in HF independent of GS-967 treatment. Similarly, the maximum rate of rise (dV/dt_{max}) during AP upstroke was also decreased by ≈25% in HF (Figure 1D). These effects are likely to be at least partly attributed to lower Na^+ channel availability (with the more positive diastolic V_m), but elevated intracellular [Na^+] ([Na^+]$_i$) and altered Na^+ channel expression (both known to occur in HF)[41–43] could also be involved. These effects were similar on acute I_{NaL} inhibition with GS-967. The maximum repolarization rate ($-dV/dt_{max}$) during AP phase 3 was significantly slower in HF (by ≈25%), and I_{NaL} block partially restored $-dV/dt_{max}$ and limited the difference between control and HF (≈15%). Collectively, these data are consistent with peak I_{Na} amplitude in HF being normal except for slight reduction in availability associated with the slightly depolarized diastolic V_m, and smaller AP amplitude and dV/dt_{max}, but enhanced I_{NaL} that contributes to APD prolongation and slowed repolarization.

Figure 1E and 1F show that HF myocytes also exhibited higher STV at 1 and 2 Hz, in HF versus control (4.80±0.51 versus 3.21±0.21 ms, respectively; 1 Hz pacing; P<0.01). Importantly, GS-967 treatment in HF decreased not only mean APD_{95} but also STV to control values (3.19±0.46 ms; not significant). GS-967 also decreased STV at all pacing rates in control (2.10±0.13 ms; P<0.001).

I_{NaL} Magnitude and Dynamic Changes Under AP in HF

The AP data indicate increased depolarization drive during the AP plateau and repolarization phases in HF versus control myocytes. Thus, we studied the 3 major inward plateau currents (I_{NaL}, I_{CaL}, and I_{NCX}) under physiological AP clamp. We did not measure the fast Na^+ current because of technical limitations (peak I_{Na} overlaps the capacitive transient under physiological AP clamp), but altered peak I_{Na} can contribute to pathological excitability in HF.[44] The reduced dV/dt_{max} observed (Figure 1D) would be consistent with reduced Na^+ current availability and peak I_{Na} in HF. GS-967–sensitive I_{NaL} and I_{Nife} were recorded from the same myocyte using AP-clamp sequential dissection[21,35] (Figure I in the Data Supplement) with either preserved [Ca^{2+}]$_i$ cycling (Physiol) or with [Ca^{2+}]$_i$ buffered with 10 mmol/L BAPTA in the pipette ($BAPTA_i$). Involvement of CaMKII was also tested using the selective CaMKII inhibitory peptide AIP. A previously recorded typical rabbit ventricular AP was used as voltage command in all AP-clamp experiments (ie, a

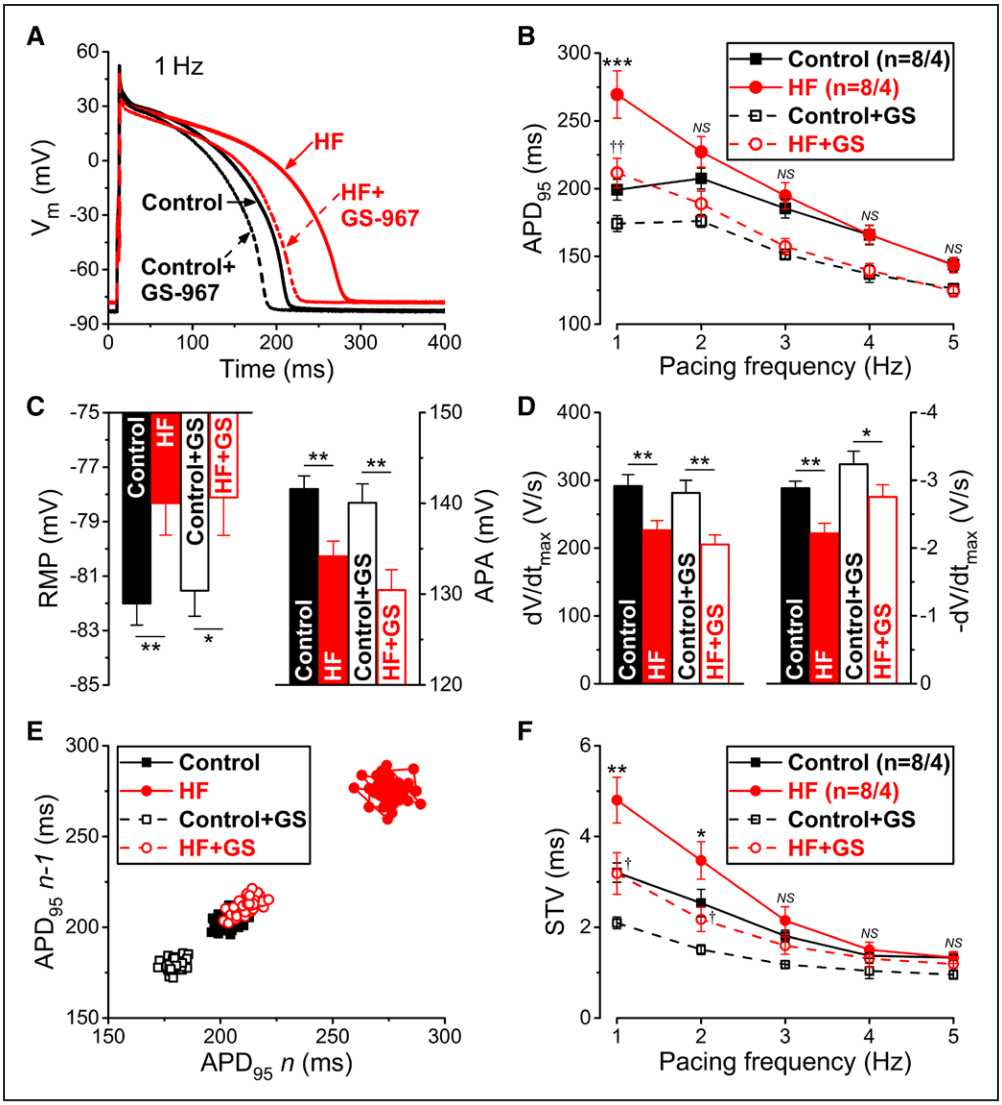

Figure 1. Frequency-dependent effects of late Na+ current inhibition on action potential (AP) in heart failure (HF).
A, Representative APs recorded at 1 Hz steady-state pacing in HF and age-matched control before and after treatment with the selective late Na^+ current inhibitor GS-967 (GS; 1 μmol/L). **B**, Frequency dependence of AP duration measured at 95% of repolarization (APD_{95}). **C**, Resting membrane potential (RMP) was slightly more positive in HF in line with decreased AP amplitude (APA) at 1 Hz pacing. GS had no effect on either AP parameters. **D**, Maximal rate of rise (dV/dt_{max}) and maximal rate of phase 3 repolarization ($-dV/dt_{max}$) were significantly decreased in HF compared with control. GS increased $-dV/dt_{max}$ already in control but even more in HF. **E**, Representative Poincaré plots of 50 consecutive APD_{95} values at 1 Hz pacing. **F**, Frequency-dependent short-term variability of APD_{95} (STV). STV was increased at low pacing frequencies in HF, which was decreased with GS to the control level. Columns and bars represent mean±SEM. n refers to cells/animals measured in each group. Paired and unpaired Student *t* tests following ANOVA. **P*<0.05, ***P*<0.01, ****P*<0.001 vs control; †*P*<0.05, ††*P*<0.01 vs control+GS.

canonical AP clamp analogous to the mean for 2 Hz where HF and control APD_{95} were similar).[14] Because HF myocytes were larger (≈35% increase in cell capacitance), all reported currents are normalized to the corresponding cell capacitance.

I_{NaL} was measured as GS-967–sensitive current under AP clamp (Figure 2; see reference[21] and Figure 1 therein for additional controls and technical details).[21] The density of I_{NaL} increased during AP repolarization as the driving force for Na^+ influx increased, achieving peak density during phase 3 repolarization of the AP (at ≈−50 mV in both control and HF). Importantly, peak I_{NaL} density was 82% higher in HF versus control myocytes in our physiological condition (−0.93±0.03 versus −0.51±0.01 A/F, respectively; *P*<0.001; Figure 2A and 2D). The I_{NaL} I-V analysis reveals that I_{NaL} is increased during the entire AP without change in V_m dependence (Figure 2A, bottom). Buffering $[Ca^{2+}]_i$ with $BAPTA_i$ did not alter peak I_{NaL} density in control (−0.54±0.02 A/F; not significant; Figure 2E) but decreased peak I_{NaL} by 23% in HF (−0.72±0.03 A/F; *P*<0.001; Figure 2B). Nevertheless, I_{NaL} density and integral charge were still larger in HF versus control myocytes with $BAPTA_i$ (Figure 2E and 2F). AIP pretreatment (to inhibit CaMKII) decreased I_{NaL} in HF to the level of untreated control (−0.54±0.02 A/F; not significant; Figure 2C and 2D). However, AIP also decreased I_{NaL} in control (−0.37±0.01 A/F; *P*<0.001; Figure 2C and 2D), such that I_{NaL} was still higher in HF versus control

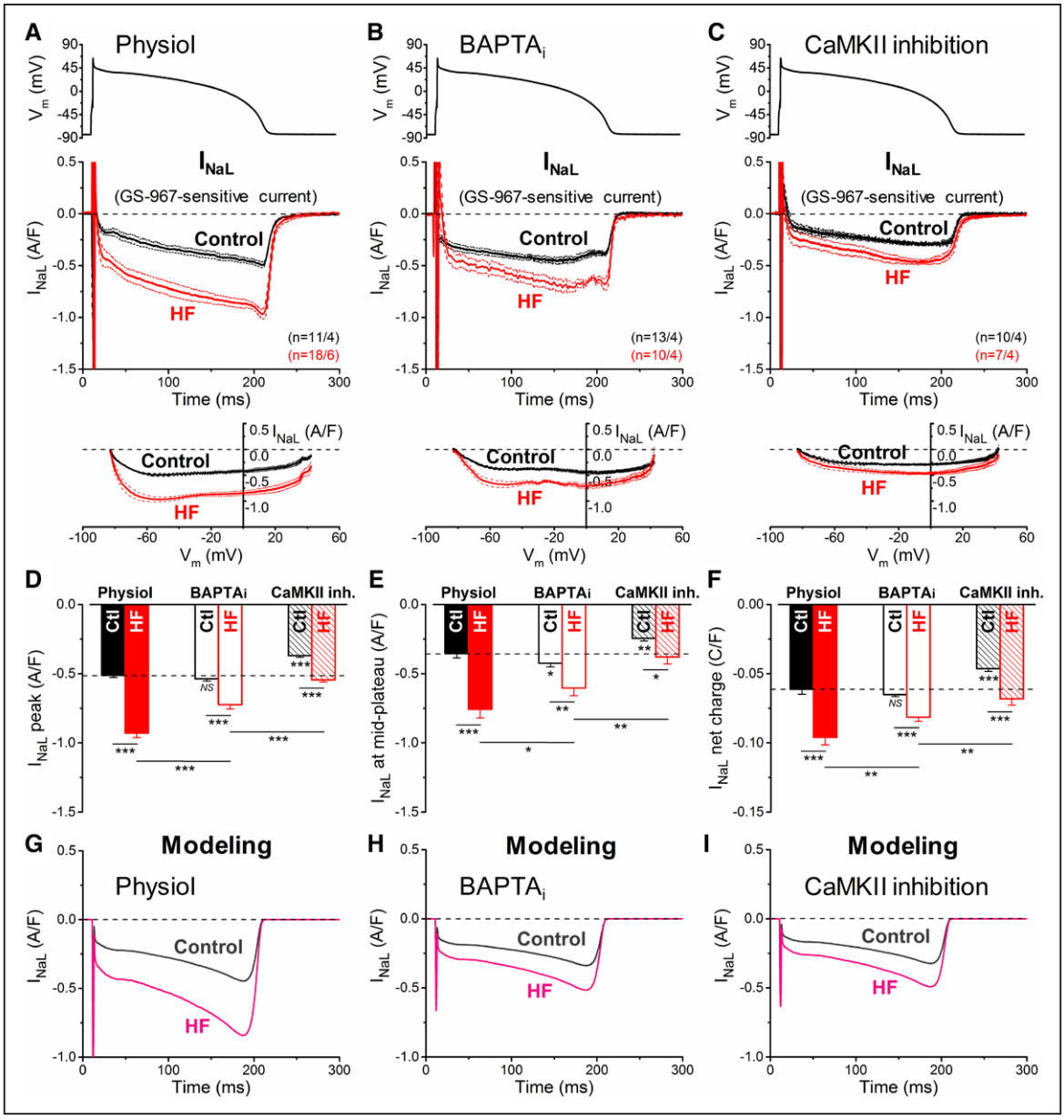

Figure 2. CaMKII (Ca2+/calmodulin-dependent protein kinase II)-dependent upregulation of late Na+ current (INaL) in heart failure (HF) under action potential (AP) clamp.

I_{NaL} was measured as GS-967 (1 µmol/L)–sensitive current in HF and age-matched control (Ctl). AP clamp using a prerecorded typical AP (shown above) was applied at 2 Hz pacing. **A**, I_{NaL} traces (mean±SEM) recorded under preserved $[Ca^{2+}]_i$ cycling (physiol). I_{NaL} was significantly increased already during the early plateau phase of the AP, and it achieved a nearly doubled peak density during phase 3 repolarization in HF cells having Ca^{2+} transients. Current-voltage relationship under AP clamp is shown below. **B**, I_{NaL} traces (mean±SEM) recorded under buffered $[Ca^{2+}]_i$ using 10 mmol/L BAPTA in the pipette ($BAPTA_i$). Buffering $[Ca^{2+}]_i$ significantly reduced I_{NaL} peak density in HF. **C**, I_{NaL} traces (mean±SEM) recorded in cells pretreated with the specific CaMKII inhibitor AIP (autocamtide-2–related inhibitory peptide; 1 µmol/L). AIP reduced I_{NaL} in HF to the untreated Ctl level; however, AIP also decreased I_{NaL} in Ctl. **D**, Peak I_{NaL} density was significantly upregulated in HF under AP, partially by a CaMKII-dependent acute effect on I_{NaL}. **E**, I_{NaL} density measured at the mid-plateau of the AP. **F**, Net charges carried by I_{NaL} under AP in HF and age-matched Ctl. Columns and bars represent mean±SEM. n refers to cells/animals measured in each group. ANOVA with Bonferroni post-test, **P*<0.05, ***P*<0.01, ****P*<0.001. **G**–**I**, Simulated time courses of I_{NaL} under AP clamp in control and HF obtained with physiol, $BAPTA_i$, and CaMKII inhibition conditions.

after AIP treatment (as for $BAPTA_i$). We conclude that I_{NaL} is elevated in HF under all conditions studied, that basal I_{NaL} at 2 Hz pacing with Ca^{2+} transients is partly dependent on CaMKII activity, and that large I_{NaL} increase in HF is substantially CaMKII dependent.

We used these data to update our most recent computational model of the rabbit ventricular myocyte.[36] The basal value of I_{NaL} maximal conductance (G_{NaL}) was scaled to 0.0527 mS/µF to reflect the peak I_{NaL} observed during the AP in control myocytes with physiological Ca^{2+} handling. Inactivation of I_{NaL} was set to 600 ms as previously.[45] G_{NaL} was modeled as a function of chronic HF-induced remodeling (not influenced by acute CaMKII inhibition, ie, 50% increase in G_{NaL} in failing versus nonfailing myocytes, guided by data in AIP-treated cells; Figure 2C), and simu-

lated CaMKII activation reproduced the increase in peak I_{NaL} observed with physiological Ca^{2+} handling versus CaMKII inhibition in both failing and nonfailing conditions, as done previously.[46] G_{NaL} (in mS/μF) was calculated as

$$G_{NaL} = 0.0527 \cdot \left(1 + 0.5 \cdot HF_{remodeling}\right) \cdot \frac{1.27}{1 + e^{-\frac{(P_{NaVs} - 0.12)}{0.1}}}$$

where $HF_{remodeling}$ indicates the absence/presence of chronic HF-induced remodeling (0 and 1, respectively), and P_{NaVs} (ranging from 0 to 1) is the fraction of phosphorylated Na^+ channels, modeled as described previously (Figure IV in the Data Supplement).[46] The in silico AP-clamp experiments quantitatively reproduced the experimental data on the role of physiological Ca^{2+} transients and CaMKII activity in upregulating I_{NaL} in control and more strongly in HF (Figure 2G through 2I).

Nifedipine-Sensitive Inward Current Changes in HF (I_{CaL} and I_{NCX})

Next, we measured I_{Nife} under AP clamp (Figure 3). Under physiological conditions, nifedipine inhibits I_{CaL} and consequently abolishes Ca^{2+} transients. Note that I_{Nife} was recorded when other Ca-sensitive currents (eg, I_{Ks}, $I_{K(Ca)}$, and $I_{Cl(Ca)}$) were pharmacologically inhibited (see Methods). Thus, the measured I_{Nife} is a composite current containing I_{CaL} and the inward shift in I_{NCX} that is driven by elevated $[Ca]_i$. Peak I_{Nife} density in the early plateau phase of the AP (at ≈+35 mV in both control and HF) was unaltered in HF versus control under physiological condition (Figure 3A and 3D). However, I_{Nife} was slightly increased in HF during the AP plateau and terminal repolarization phases (Figure 3A and 3E), potentially because of either less Ca^{2+}-dependent inactivation (CDI) of I_{CaL} in HF (due to reduced Ca^{2+} transients),[4,9] enhanced Ca^{2+}/CaMKII-dependent facilitation (CDF), altered Ca^{2+} chan-

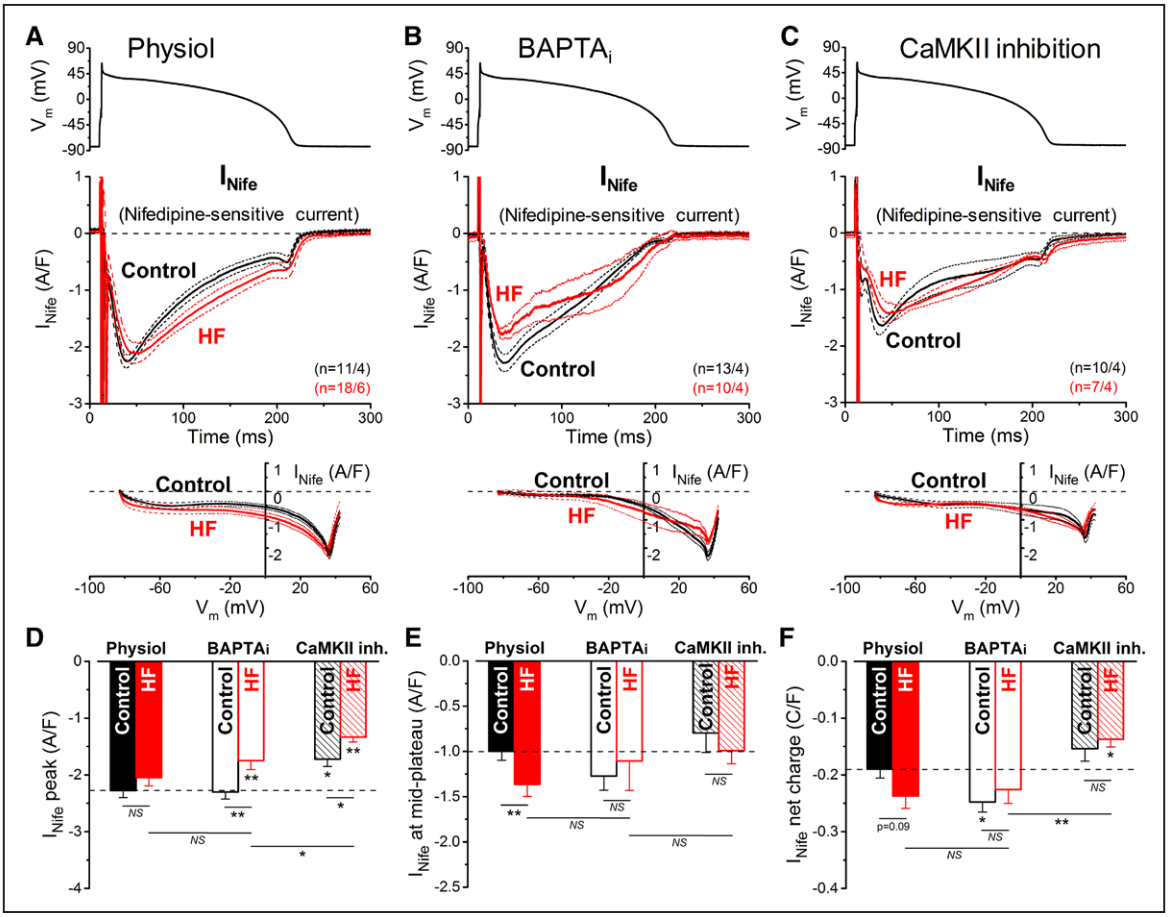

Figure 3. Nifedipine-sensitive current in heart failure (HF) under action potential (AP) clamp.
The L-type Ca^{2+} current and the inward Na^+/Ca^{2+} exchange current under AP were measured as a composite nifedipine-sensitive current (I_{Nife}) in HF and age-matched control. AP clamp using a prerecorded typical AP (shown above) was applied at 2 Hz pacing before and after application of 10 μmol/L nifedipine (Nife). **A**, I_{Nife} traces (mean±SEM) recorded under preserved $[Ca^{2+}]_i$ cycling (physiol). I_{Nife} was increased during the mid-plateau and the late-plateau phases of the AP in HF. Current-voltage relationship under AP clamp is shown below. I_{Nife} traces (mean±SEM) recorded under buffered $[Ca^{2+}]_i$ using 10 mmol/L BAPTA in the pipette ($BAPTA_i$). Buffering $[Ca^{2+}]_i$ significantly reduced I_{Nife} peak density in HF. **C**, I_{Nife} traces (mean±SEM) recorded in cells pretreated with the specific CaMKII (Ca^{2+}/calmodulin-dependent protein kinase II) inhibitor AIP (autocamtide-2–related inhibitory peptide; 1 μmol/L). AIP slightly reduced I_{Nife} peak density in HF. **D**, Peak I_{Nife} density was significantly upregulated in HF under AP by CaMKII. **E**, I_{Nife} density measured at the mid-plateau of the AP. **F**, Net charges carried by I_{Nife} under AP in HF and age-matched control. Columns and bars represent mean±SEM. n refers to cells/animals measured in each group. ANOVA with Bonferroni post-test, *P<0.05, **P<0.01, ***P<0.001.

nel subunit composition, or alternatively, but less likely,[41] to more inward I_{NCX}. In contrast, when I_{Nife} was recorded with $BAPTA_i$ (ie, without Ca^{2+} transient and inward I_{NCX}), peak I_{Nife} density (more exclusively I_{CaL}) under AP clamp was significantly decreased in HF (Figure 3B and 3D), but BAPTA also abolished the small hump near terminal repolarization, consistent with loss of expected inward I_{NCX} at this time (note superimposition of I_{Nife} versus V_m curve between –80 and –40 mV). In $BAPTA_i$, the I_{Nife} decay was still slower in HF versus control, despite low CDI expected in both cases (Figure 3B and 3E). When CaMKII was inhibited, the I_{Nife} density and integrated charge movement were reduced versus Physiol for both HF and control (Figure 3C, 3D, and 3F). Because the peak inward I_{Nife} is likely dominated by peak I_{CaL}, this might reflect the involvement of basal CaMKII activity in maintaining physiological peak I_{CaL} when Ca^{2+} transients and CaMKII are functional (Figure 3A and 3D).

Changes in the Biophysical Properties of I_{CaL} in HF

Next, we measured the biophysical parameters of I_{CaL} using conventional square-pulse voltage clamp and $[Ca^{2+}]_i$ buffered to 100 nmol/L by inclusion of 5 mmol/L EGTA in the pipette solution. The peak density of I_{CaL} and the I-V relationship were not significantly different (Figure 4A), but the steady-state activation curve of I_{CaL} was shifted slightly (4.7 mV) to more negative potentials in HF versus control (Figure 4B). The inactivation time constants of I_{CaL} (obtained by biexponential fits of I_{CaL} decay) were slightly prolonged in HF versus control, consistent with slower CDI in HF (Figure 4D and 4E), but V_m dependence of inactivation (Figure 4C) and the recovery from inactivation kinetics (Figure 4F) were unchanged.

We also analyzed I_{CaL} in the pipette conditions used for AP-clamp studies (Physiol, $BAPTA_i$, and CaMKII inhi-

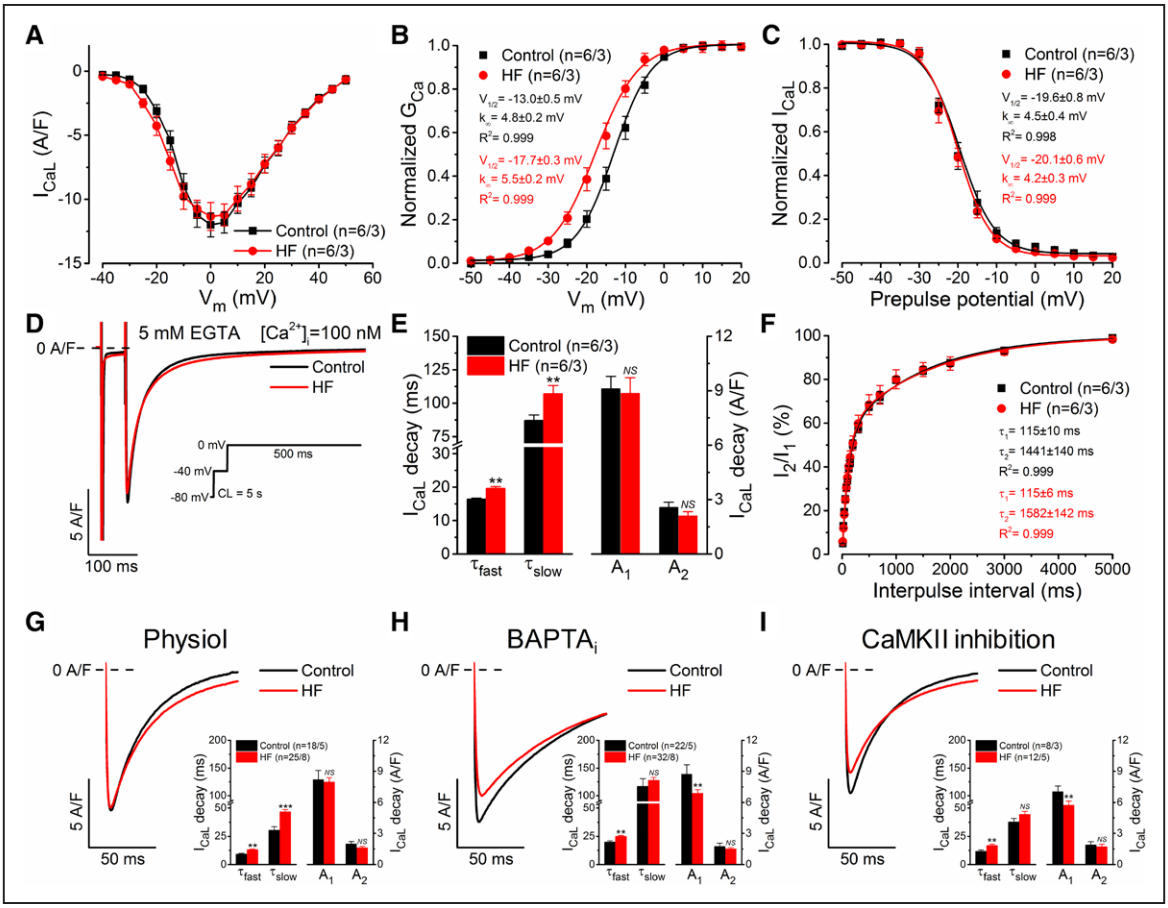

Figure 4. Biophysical properties of L-type Ca2+ current (ICaL) in heart failure (HF).
A, Current-voltage relationship of I_{CaL} peak density in HF and age-matched control. I_{CaL} was measured in the presence of 5 mmol/L EGTA ($[Ca^{2+}]_i$=100 nmol/L) in the pipette. **B**, Steady-state activation of I_{CaL} was shifted by 5 mV to more negative potentials in HF. **C**, Steady-state inactivation of I_{CaL} was unaltered in HF. **D**, Representative I_{CaL} traces elicited by depolarization pulses to 0 mV (voltage protocol shown in the inset). **E**, Decay time constants (τ_{fast} and τ_{slow}) of I_{CaL} were slightly increased in HF. **F**, I_{CaL} recovery from inactivation was unchanged in HF. **G**, Representative I_{CaL} traces under preserved $[Ca^{2+}]_i$ cycling (physiol). I_{CaL} was elicited with depolarization pulse to 0 mV at 2 Hz. Inset shows significantly increased decay time constants but unaltered I_{CaL} amplitude in HF. **H**, Representative I_{CaL} traces under buffered $[Ca^{2+}]_i$ using 10 mmol/L BAPTA in the pipette ($BAPTA_i$). Inset shows that the amplitude of the fast I_{CaL} decay was significantly reduced in HF vs control, whereas τ_{fast} was still slightly increased in HF. **I**, Representative I_{CaL} traces following specific CaMKII (Ca^{2+}/calmodulin-dependent protein kinase II) inhibition with AIP (autocamtide-2–related inhibitory peptide; 1 μmol/L). Inset shows the decay time constants of I_{CaL} and the corresponding amplitudes. The inactivation time course of I_{CaL} was fitted by a biexponential function. Columns and bars represent mean±SEM. n refers to cells/animals measured in each group. ANOVA with Bonferroni post-test, *P<0.05, **P<0.01, ***P<0.001.

bition). Peak I_{CaL} density elicited by a step pulse to 0 mV was unaltered in HF versus control with preserved $[Ca^{2+}]_i$ cycling (Figure 4G). This contrasts with the diminished peak I_{CaL} observed when either $[Ca^{2+}]_i$ is clamped low ($BAPTA_i$) or CaMKII is inhibited (Figure 4H and 4I), both conditions where CaMKII-dependent CDF is suppressed. We infer that Ca^{2+}-dependent CaMKII upregulates peak I_{CaL} (via CDF) in HF to the level of control cells (when measured in physiological conditions; compare Figure 4G through 4I).

CDI of I_{CaL} was, as expected, stronger under physiological $[Ca^{2+}]_i$ versus when $[Ca^{2+}]_i$ was buffered by EGTA or BAPTA (Figure 4G versus Figure 4E and 4H). However, the τ of inactivation was significantly slowed in HF versus control (Figure 4G, inset), consistent with known smaller Ca^{2+} transients in HF and thus less CDI.[4,9] Using 10 mmol/L BAPTA in the pipette ($BAPTA_i$) should eliminate both CDI and CDF (Figure 4H). Indeed, $BAPTA_i$ significantly slowed the τ of inactivation (versus Physiol or EGTA; Figure 4H and 4I) but τ_{fast} was still slightly slower in HF versus control (Figure 4H, inset). When CaMKII was inhibited with AIP (Figure 4I), the inactivation τ values were more like those in physiological buffer (Figure 4G). The slowed I_{CaL} inactivation in HF was still observable in BAPTA, consistent with part of that effect being independent of CDI, and may reflect some PKA-dependent effect in HF myocytes.[47,48]

Computer Models Help to Report Physiological I_{CaL} and I_{NCX} During the AP in HF

To help delineate the relative contributions of I_{CaL} and I_{NCX} to I_{Nife} under AP clamp, we used our rabbit ventricular myocyte model[36] with I_{CaL} properties tuned to those measured in Figure 4 (for details, see Methods, Table I in the Data Supplement, and Figure II in the Data Supplement). Figure 5 shows how in silico experiments can inform the distinct profiles of I_{CaL} and I_{NCX} under AP clamp in control and HF cells under physiological Ca^{2+} transients (Figure III in the Data Supplement). Figure 5A and 5B shows calculated I_{CaL} and $I_{Na/Ca}$ in physiological conditions, which have the expected overall shapes.[10,37,41,49,50] After I_{CaL} activation and the start of SR Ca^{2+} release, CDI causes I_{CaL} decline to a plateau that can increase slightly as AP repolarization causes an increase in the Ca^{2+} driving force, until terminal repolarization deactivates I_{CaL}. I_{NCX} is initially outward (Ca^{2+} influx) driven by the rapid AP depolarization. But once SR Ca^{2+} release occurs, the high submembrane $[Ca^{2+}]_i$ drives a first peak of inward I_{NCX}, which declines as $[Ca^{2+}]_i$ falls but is followed by a second peak during terminal repolarization (driven by voltage) until the $[Ca^{2+}]_i$ reaches the diastolic level. In HF, the I_{CaL} waveform is similar, although CDI is slowed. The higher $[Na^+]_i$ and smaller Ca^{2+} transient in HF shifts the I_{NCX} waveform outward during the plateau, and the higher NCX expression levels cause the larger inward I_{NCX} tail on final repolarization.[10,41]

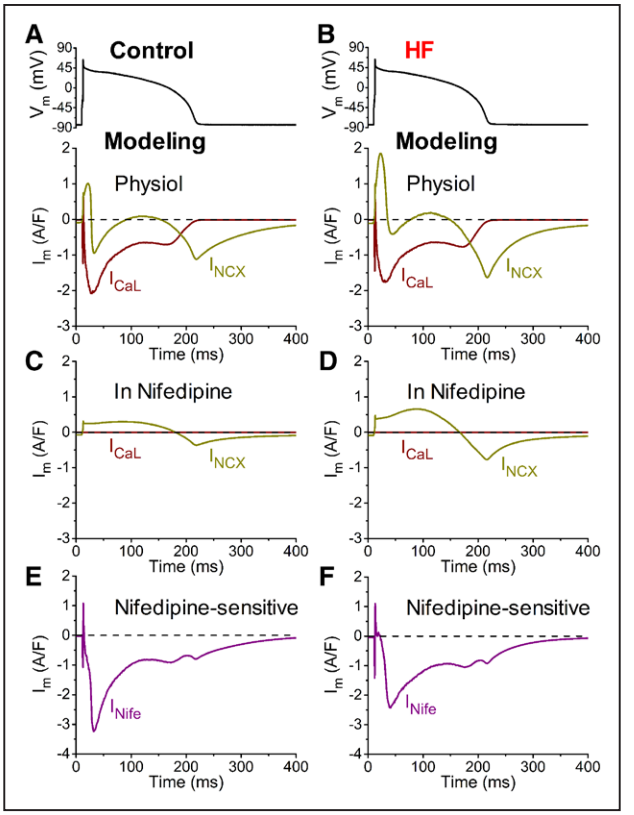

Figure 5. Simulated time courses of L-type Ca2+ current (ICaL) and Na+/Ca2+ exchanger current (INCX) under action potential (AP) clamp in heart failure (HF).
Simulated I_{CaL} and I_{NCX} have been obtained with our updated rabbit ventricular myocyte model that integrates detailed descriptions of electrophysiology, Ca^{2+} and Na^+ handling, PKA (protein kinase A) and CaMKII (Ca^{2+}/calmodulin-dependent protein kinase II) signaling, and myofilament contraction. **A** and **B**, Simulated I_{CaL} and I_{NCX} under AP clamp at 2 Hz pacing in control (**left**) and HF (**right**) with physiological Ca^{2+} handling. **C** and **D**, Simulated I_{CaL} and I_{NCX} after nifedipine (Nife) treatment (simulated assuming complete block of I_{CaL}) under AP clamp at 2 Hz pacing in control and HF. **E** and **F**, Nifedipine-sensitive current (I_{Nife}) expressed as sum of the changes in simulated I_{CaL} and I_{NCX} before and after nifedipine treatment in control and HF.

Figure 5C and 5D shows how I_{CaL} and I_{NCX} are expected to change after 3 minutes of nifedipine exposure, which blocks I_{CaL} and SR Ca^{2+} release. Without I_{CaL} or SR Ca^{2+} release, the AP drives outward I_{NCX} (Ca^{2+} influx) throughout much of the AP, and then that same amount of Ca^{2+} that entered via outward I_{NCX} is extruded via inward I_{NCX} during repolarization. Higher NCX expression in HF myocytes makes inward and outward I_{NCX} larger in HF. The residual I_{NCX} during nifedipine exposure must be taken into account when inferring the predicted I_{Nife} shown in Figure 5E and 5F. The shape of the predicted I_{Nife} is similar to the I_{Nife} recorded in vitro under AP clamp in cardiomyocytes (Figure 3A). This analysis also explains why the inward I_{NCX} tail at terminal repolarization is less prominent than expected in the measured I_{Nife} traces in Figure 3A and

3C. Although this simulation analysis cannot extract absolute I_{CaL} and I_{NCX} waveforms that occur during the AP in control versus HF myocytes, Figure 5A provides a qualitative estimate of likely changes that occur in I_{CaL} and I_{NCX} during the HF AP.

Altered β-Adrenergic Response of Inward Currents in HF

Elevated sympathetic tone is often reported in HF in conjunction with altered responses to βAR activation. We, therefore, tested the effects of acute βAR stimulation on I_{NaL} and I_{Nife} in HF versus control myocytes using AP clamp. Because downstream effects of βAR stimulation are mediated both by PKA and CaMKII and the activities of these kinases are known to be altered in HF, ionic currents were measured again with physiological preserved $[Ca^{2+}]_i$ cycling and with heavily buffered $[Ca^{2+}]_i$.

Figure 6A shows I_{NaL} measured after βAR agonist ISO (10 nmol/L) treatment. ISO increased I_{NaL} in both control and HF myocytes but by a much larger percentage in control (by 110% versus 40%; Figure 6C). Nevertheless, the resulting I_{NaL} with ISO (and its integral) was still larger in HF. Buffering $[Ca^{2+}]_i$ reduced the effect of ISO on I_{NaL}, indicating the involvement of Ca^{2+} and CaMKII (as well as PKA) in mediating the ISO effect. Again, the effect on control was larger than in HF (70% versus 30%). Moreover, in $BAPTA_i$, the ISO-induced I_{NaL} peak density was not significantly different between control and HF. That is consistent with Ca^{2+} or CaMKII dependence being

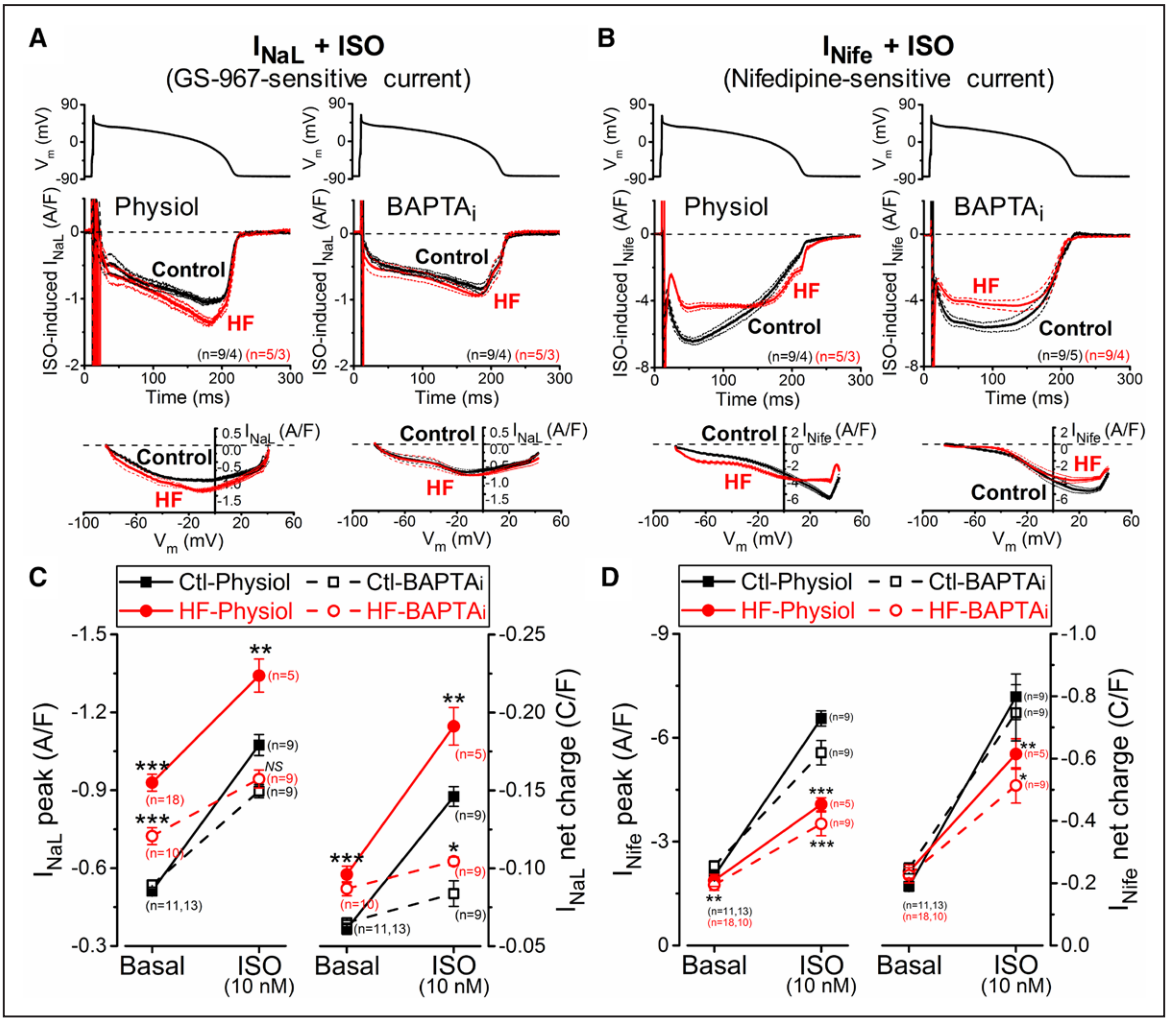

Figure 6. Altered response of inward currents to βAR (β-adrenergic receptor) stimulation in heart failure (HF).
The late Na^+ current (I_{NaL}) and the nifedipine-sensitive current (I_{Nife}) were recorded after 2-min pretreatment with βAR agonist isoproterenol (ISO; 10 nmol/L). **A**, I_{NaL} traces (mean±SEM) under action potential (AP) clamp at 2 Hz pacing measured with preserved $[Ca^{2+}]_i$ cycling (physiol) and $[Ca^{2+}]_i$ buffering using 10 mmol/L BAPTA in the pipette ($BAPTA_i$) after ISO pretreatment in HF and age-matched control (Ctl). Current-voltage relationship under AP clamp is shown below. **B**, I_{Nife} traces (mean±SEM) under AP clamp after ISO pretreatment in HF and age-matched Ctl. **C**, Upregulation of I_{NaL} peak and net charge induced by ISO, which was reduced with $BAPTA_i$. **D**, Robust increase in I_{Nife} after ISO stimulation, which was reduced in $BAPTA_i$, indicating a Ca^{2+}-dependent pathway in mediating the response of βAR stimulation on I_{Nife} (besides the classical protein kinase A effect). HF cells exhibited significantly reduced response of I_{Nife} after ISO stimulation both with and without $[Ca^{2+}]_i$ buffering. Symbols and bars represent mean±SEM. n refers to cells measured in each group, and the cells in each group came from 3 to 6 individual animals. ANOVA with Bonferroni post-test, $*P<0.05$, $**P<0.01$, $***P<0.001$.

involved with ISO-induced higher I_{NaL} in HF versus control.

I_{Nife} also increased after ISO treatment, as expected for the known effects of βAR stimulation on I_{CaL} and Ca^{2+} transient amplitude (which drives inward I_{NCX}; Figure 6B). Again, the ISO-induced increase in I_{Nife} was smaller in HF. This blunted βAR response in HF was present with both physiological Ca^{2+} cycling and $BAPTA_i$ conditions, but for I_{Nife}, the ISO-induced increase for $BAPTA_i$ (2.4-fold in control versus 2-fold in HF) was only slightly smaller than for physiological conditions (3.3-fold in control versus 2.2-fold increase in HF; Figure 6D).

Because the ISO effects on both I_{NaL} and I_{Nife} were blunted in HF versus control, we tested whether this was because of decreased ISO sensitivity or limited maximal response. ISO concentrations between 3 and 300 nmol/L were applied in HF and control (Figure 7). Steady-state contracting AP-clamped myocytes in HF were unstable at higher ISO concentrations; so these experiments were performed with 10 mmol/L BAPTA in the pipette ($BAPTA_i$). ISO increased I_{NaL} in both control and HF, but the half maximal effective concentration [ISO] was slightly higher in HF (16.1±1.4 versus 10.5±1.3 nmol/L; $P<0.05$; Figure 7A). However, the maximal ISO-induced I_{NaL} density was not different in control versus HF (Figure 7A). I_{CaL} was also markedly increased after ISO application with similar half maximal effective concentration (≈12 nmol/L) in control and HF. However, the maximal I_{CaL} response after ISO stimulation was only half as much in HF versus control (4.6- versus 2.7-fold increase in peak I_{CaL}; Figure 7B). This indicates unchanged ISO sensitivity but weaker potency in raising I_{CaL}. The blunted ISO response of I_{CaL} in HF may limit Ca^{2+} transients and inotropy in HF during sympathetic activity.

Relative Contributions of Inward Currents to AP Plateau and Phase 3 Repolarization

The dynamic interplay of time- and voltage-dependent activation and inactivation of inward currents governs the AP waveform. Each inward current has a unique profile and magnitude during the cardiac AP. The relative contributions of major inward currents (I_{NaL}, I_{Nife}≈I_{CaL}+I_{NCX}) during the AP plateau and repolarization in control and in HF are shown in Figure 8, compared at different V_m (+40, −20, and −60 mV), and shown as integrated charge movement during the AP (Figure 8, insets). I_{Nife} early in the AP (phase 1, at +40 mV) predominantly represents I_{CaL}, whereas late during terminal repolarization (at −60 mV) is mainly inward I_{NCX} (during physiological Ca^{2+} transients).

Total inward current during AP phase 1 (early repolarization) was unaltered in HF versus control in physiological conditions but had greater I_{NaL} contribution in HF (Figure 8A and 8B). Later during AP repolarization (−20 and −60 mV), total inward current was higher in HF, mainly because of increased I_{NaL} (Figure 8B). In control myocytes, ISO increased both inward currents, but the smaller ISO-induced increases of I_{CaL} in HF reduced I_{CaL} throughout the AP (Figure 8C). Total inward current in HF was reduced early (+40 mV) but increased progressively later in the AP (−20 and −60 mV), which could promote failure of repolarization and EADs. Despite βAR hyporesponsiveness, I_{NaL} and I_{NCX} were still higher in HF and contributed to that increased total inward current late in the AP (with ISO).

In contrast to physiological conditions, CaMKII inhibition limited both I_{NaL} and I_{Nife} increases in HF and abolished differences in late AP total inward current

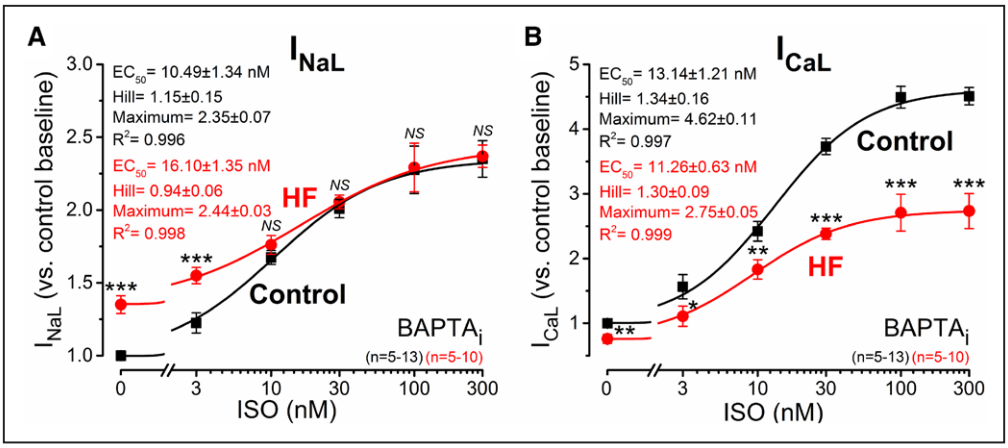

Figure 7. βAR (β-adrenergic receptor) responsiveness of inward currents in heart failure (HF).
Dose-response effect of isoproterenol (ISO) on late Na^+ current (I_{NaL}) and L-type Ca^{2+} current (I_{CaL}) peak densities under action potential clamp at 2 Hz pacing rate. Pipette solution contained 10 mmol/L BAPTA ($BAPTA_i$). **A**, I_{NaL} measured as GS-967–sensitive current significantly increased after ISO application. I_{NaL} sensitivity (half maximal effective concentration [EC_{50}]) to ISO was slightly reduced in HF, and I_{NaL} exhibited similar maximal response in HF than in control, despite the increased basal I_{NaL} in HF. **B**, I_{CaL} measured as nifedipine-sensitive current was markedly increased after ISO treatment; however, the magnitude of the response was significantly blunted in HF with no change in ISO sensitivity. EC_{50} values, Hill coefficients, and maximum responses were determined by fitting data to the Hill equation, indicated by solid lines. Symbols and bars represent mean±SEM. n refers to the number of cells measured in each group, and the cells in each group came from 3 to 6 individual animals. ANOVA with Bonferroni post-test, *$P<0.05$, **$P<0.01$, ***$P<0.001$.

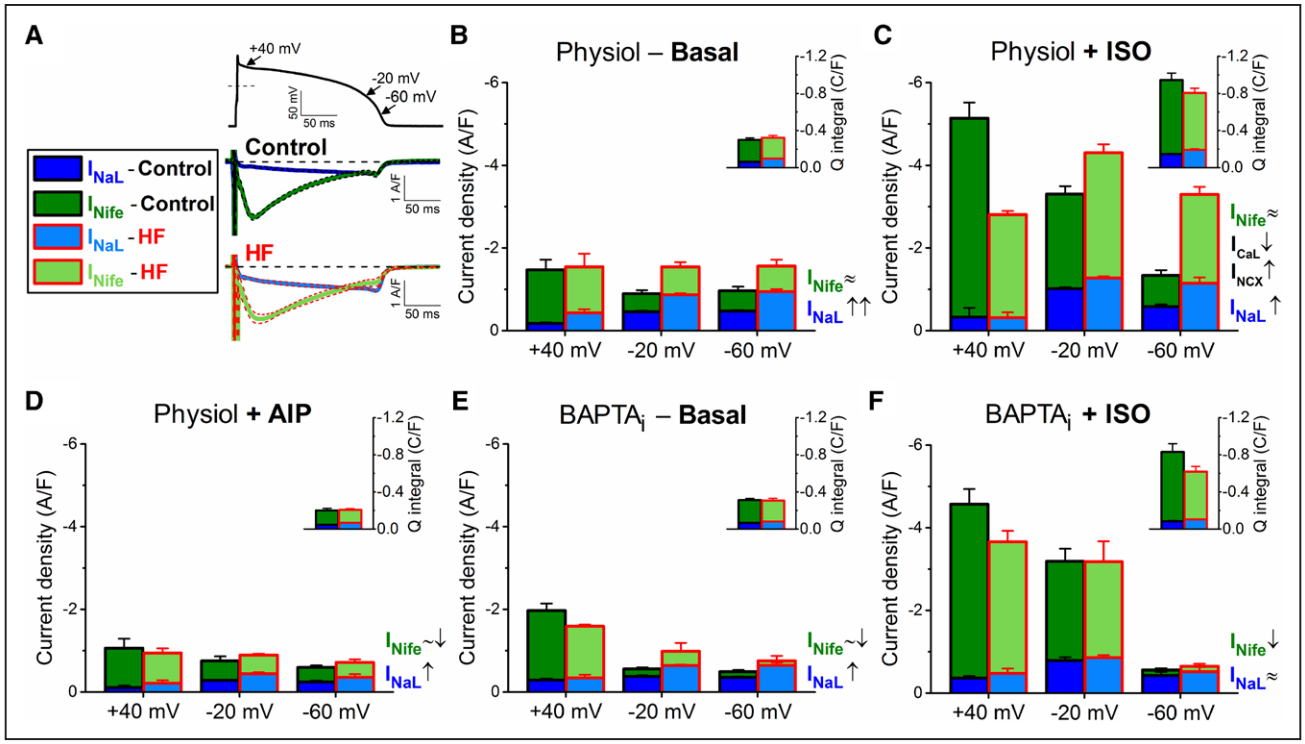

Figure 8. Relative contribution of inward currents to net depolarizing current in heart failure (HF).
Relative contributions and magnitudes of the major inward currents (late Na^+ current [I_{NaL}] and nifedipine-sensitive current [I_{Nife}]) are compared in distinct phases of the action potential (AP) repolarization process in HF to those in age-matched control. Magnitude of I_{Nife} at the early repolarization phase (phase 1) of the AP (at +40 mV) predominantly represents L-type Ca^{2+} current (I_{CaL}), whereas the magnitude of I_{Nife} during the terminal repolarization (at –60 mV) is generated predominantly by the inward Na^+/Ca^{2+} exchanger current (I_{NCX}; under physiological conditions). **A**, I_{NaL} and I_{Nife} traces measured in control and HF under AP clamp at 2 Hz pacing without using any Ca^{2+} buffer or βAR (β-adrenergic receptor) agonist. Mean traces and SEM are shown. **B**, When $[Ca^{2+}]_i$ cycling is preserved, upregulation of I_{NaL} increased the net inward current during phase 3 of AP. **C**, βAR stimulation using isoproterenol (ISO; 10 nmol/L) significantly upregulated not only I_{CaL} but also I_{NaL} and I_{NCX}. However, HF cells were hyporesponsive to ISO-induced stimulation (ie, both I_{CaL} and I_{NaL} increased in a smaller extent than in control); thus net inward current at +40 mV (predominantly I_{CaL}) was significantly decreased in HF compared with control. Despite hyporesponsiveness, the net inward current during AP terminal repolarization was still significantly increased in HF because of the upregulated I_{NaL} and I_{NCX}. **D**, CaMKII (Ca^{2+}/calmodulin-dependent protein kinase II) inhibition using the specific inhibitory peptide AIP (autocamtide-2–related inhibitory peptide) largely diminished the difference between control and HF by reducing the upregulated I_{NaL} in HF. **E**, Buffering $[Ca^{2+}]_i$ ($BAPTA_i$) eliminated the inward I_{NCX} and significantly decreased the extent of I_{NaL} enhancement in HF limiting the increase in net inward current. **F**, Under βAR stimulation in $BAPTA_i$, HF cells exhibited slightly decreased I_{CaL} but similar I_{NaL} density compared with control. The contributions of these inward currents to total net charge are shown in insets. Columns and bars represent mean±SEM. Statistics and n numbers are shown in Figures 2 through 6.

between HF and control (Figure 8D versus Figure 8B). Similarly, using strong $[Ca^{2+}]_i$ buffering also reduced I_{NaL} and I_{Nife} in HF, and total inward current was unaltered early but still slightly increased late during the AP in HF versus control (Figure 8E). ISO did not change total inward current during phase 3 of the AP in the presence of $BAPTA_i$ (presumably because inward I_{NCX} is prevented; Figure 8F).

DISCUSSION

Arrhythmogenic AP Alterations in HF and the Role of Increased I_{NaL}

HF-induced ionic remodeling causes characteristic changes in ventricular AP profile in our rabbit HF model, including APD prolongation, reduction of phase 1 and phase 3 repolarization rates, depolarized resting membrane potential, and reduced AP upstroke velocity under steady-state pacing (Figure 1A through 1D), which mostly agree with literature data on various animal HF models and human HF.[4–7,18,25,26,51] Moreover, temporal variability of AP repolarization (characterized by STV) was also increased in HF (Figure 1E and 1F), further enhancing the arrhythmogenic substrate.[6–8] Delayed afterdepolarizations are frequently reported in HF,[3,4] and we have shown previously increased delayed afterdepolarizations that depended on CaMKII-mediated SR Ca^{2+} leak after cessation of pacing bouts in this HF model.[14,52,53]

The HF-related arrhythmogenic alterations in ventricular AP were more pronounced at slow pacing rates than at fast pacing rates (Figure 1) in line with previous experimental[14,54] and clinical data.[55] Importantly, selective I_{NaL} inhibition in HF reduced both APD and STV to control values at all pacing rates. The rate dependence of APD prolongation and increase in STV associated with enhanced I_{NaL} in HF can be explained by the following mechanisms: (1) I_{NaL} availability may decrease at faster pacing rates[56]; (2) amplitude of Ca^{2+} transients may decrease at faster pacing rates in HF cells unlike healthy control, altering the magnitude of Ca^{2+}-dependent ionic currents and I_{NCX}[57]; (3) the delayed rectifier

K^+ currents that counterbalance I_{NaL} during AP plateau and phase 3 are also increased in HF under physiological conditions at faster pacing rates,[14] and the increase of those K^+ currents has also been shown to be Ca^{2+}/CaMKII dependent.[14]

In line with our results in HF rabbits, it has been shown that both the I_{NaL} inhibitor ranolazine and AIP exert potent antiarrhythmic effects in a transverse aortic constriction (pressure overload)–induced HF model in mice,[18] as well as in failing human myocytes.[24] Inhibition of the enhanced I_{NaL} prevented APD prolongation and STV enhancement in our rabbit HF model; thus, it reduced the substrate for arrhythmias. Moreover, enhanced I_{NaL} can also contribute to increased Na^+ loading and (via NCX) Ca^{2+} loading and contribute to increased occurrence of afterdepolarizations that triggers arrhythmias in HF.[23] Furthermore, enhanced Na^+ current and spontaneous SR Ca^{2+} leak can contribute to increased STV.[33,58] Of note, the I_{NaL} maximal conductance used in the mathematical model to fit our AP-clamp current data is ≈10-fold larger than previously estimated in rabbit myocyte experiments using a different experimental approach (1-day cell culture, square voltage pulses to −20 mV, abolished Ca^{2+} cycling).[45] Physiologically dynamic Ca^{2+}-dependent CaMKII activation and AP shape may contribute to these differences, which underlines the importance of using physiological AP clamp to measure ionic currents.

Changes in Inward Currents in HF That Shape the AP

Electrophysiological remodeling in HF leads to arrhythmogenic alterations in AP morphology that involves changes in the expression and regulation of multiple ion channels.[26] Experimental data detailing such changes have been integrated in computational models to understand mechanistically how arrhythmogenesis occurs in HF.[40,59] However, ionic currents were usually recorded under nonphysiologic conditions, which may mask modulation by Ca^{2+} transients and CaMKII on ionic currents. This regulation may be even more impactful under pathological states, including HF (where CaMKII activity is increased).[14,52,60] Accordingly, we have shown that Ca^{2+} transient, CaMKII, and βAR stimulation regulates K^+ currents under physiological AP clamp and importantly, that this regulation was significantly altered in HF.[14] Importantly, Ca^{2+}/CaM and CaMKII are also known to regulate both Na^+ and Ca^{2+} channels. Ca^{2+}/CaM binding to the IQ motif of these channels is known to enhance CDI that is evident, especially for I_{CaL},[61,62] but a similar mechanism has been shown for fast I_{Na} and I_{NaL}.[63,64] CDI serves as a feedback mechanism preventing cellular Ca^{2+} overload.[29] In contrast, CaMKII increases both I_{CaL} (via CDF)[27–29] and I_{NaL}.[17,64]

I_{NaL} represents a noninactivating or slowly inactivating component of Na^+ current that persists throughout the AP plateau and phase 3, as shown in Figure 2. The gating mechanisms contributing to I_{NaL} have been extensively studied and may include the early burst and late scattered openings, nonequilibrium gating, and steady-state window current (overlap between the activation and inactivation curves); however, the details are still not fully resolved.[65] I_{NaL} enhancement in HF has been demonstrated in different animal models and human[11,12]; however, we found an even more pronounced increase in I_{NaL} under physiological AP clamp than previous reports of smaller I_{NaL} under nonphysiological voltage-clamp conditions.[11,17,19,45,56] We showed that I_{NaL} upregulation in HF was largely Ca^{2+} dependent (Figure 2), in line with the increased CaMKII activity in HF that upregulates I_{NaL}.[17–19] However, I_{NaL} was still increased in HF following cytosolic Ca^{2+} buffering with BAPTA, potentially reflecting an increased basal PKA-dependent phosphorylation of Na^+ channels or remodeling with increased expression of neural Na^+ channel isoforms in HF.[42,43]

I_{CaL} is the main inward current during the AP plateau in ventricular cardiomyocytes, as shown in Figure 3. I_{CaL} amplitude was unchanged in HF under physiological conditions or using the slow Ca^{2+} buffer EGTA (which does not eliminate subsarcolemmal $[Ca^{2+}]$ changes; Figure 4). In contrast, I_{CaL} was slightly decreased in HF when measured with $BAPTA_i$ and AIP, indicating a key role of CaMKII in maintaining I_{CaL} in HF. I_{CaL} decay was significantly slower in HF. This might be explained by reduced CDI (because of reduced Ca^{2+} transient amplitude), enhanced CDF (via increased CaMKII activity), or altered Ca^{2+} channel subunit composition. Increased expression of auxiliary β_2 subunit is known to occur in HF,[66] and it has been shown to reduce the rate of I_{CaL} inactivation, shift activation to more negative potentials, and significantly diminishes PKA response, all in agreement with our data.[67–69]

The difference in nifedipine-sensitive inward current measured with and without $[Ca^{2+}]_i$ buffering suggests enhanced I_{NCX}, in agreement with previous reports.[9] I_{NCX} kinetics during the rabbit ventricular AP during Ca^{2+} transients was previously measured in an elegant study of Weber et al.[49] Here, we could not explicitly separate I_{NCX} from I_{Nife} (Figure 3), but our measurements of I_{CaL} alone (Figure 4) and in silico models (Figure 5) were consistent with the upregulation of NCX previously reported in this HF model. Our modeling provided quantitative estimates of I_{NCX} dynamics under AP clamp in control and HF (Figure 5). Importantly, the increased I_{NCX} peak during phase 3 of AP repolarization in HF may contribute to early afterdepolarizations and APD prolongation. However, the precise contribution of I_{NCX} to arrhythmogenic AP alterations in HF requires further studies.

β-Adrenergic Stimulation–Induced Changes in Inward Currents in HF

Increased sympathetic activity but blunted β-adrenergic response are hallmarks of HF and significantly contribute to contractile dysfunction, alterations in Ca^{2+} handling system, and arrhythmogenesis.[4,14,52,70,71]

I_{CaL}, I_{NaL}, and I_{NCX} are all known to be increased in ventricular myocytes after βAR stimulation. Downstream signaling mediating βAR effects on Na^+ and Ca^{2+} channels involves both PKA and CaMKII; however, there is still debate on the exact molecular mechanisms and phosphorylation sites.[72,73] We found that I_{CaL} peak was upregulated mainly by PKA during ISO stimulation (by comparing physiological and $BAPTA_i$ conditions), whereas I_{NaL} was upregulated by PKA and CaMKII in an almost equal manner both in control and HF (Figure 6). Importantly, the ISO-induced increases in I_{CaL} and I_{NaL} were limited in HF both in physiological and $BAPTA_i$ conditions (Figure 6). While the ISO half maximal effective concentration for I_{NaL} activation was slightly increased in HF, the eventual maximal I_{NaL} density was the same in HF versus age-matched control, in part, because of the increased basal I_{NaL} in HF (Figure 7A). On the contrary, the ISO half maximal effective concentration for I_{CaL} activation was not altered in HF, but the maximal effect was ≈40% smaller in HF versus age-matched control (Figure 7B) similar to prior report in this HF model.[4] This blunted βAR response could be because of reduced number of β_1ARs,[70] lower local cAMP levels,[71] or altered phosphatases and phosphodiesterases in HF.[52]

I_{CaL}, I_{NaL}, and I_{NCX} reach their peak density sequentially during the AP, and their relative contributions to net inward current also dynamically change during the AP time course, as demonstrated previously in pig[51] and guinea pig[20,31] cardiomyocytes. In this study, we demonstrated their detailed contribution in a chronic pressure/volume overload–induced HF rabbit model (Figure 8). The enhanced I_{NaL} and I_{NCX} increase the demand on the repolarizing K^+ currents, which are also remodeled in HF.[13,14] The balance between these depolarizing and repolarizing currents in HF is shifted during phase 3 of the AP so as to slow repolarization and prolong APD.[51]

Conclusions

We measured I_{NaL} under physiological recording conditions (AP clamp with physiological ionic composition, pacing rate, $[Ca^{2+}]_i$, and temperature) and demonstrated a key role I_{NaL} enhancement in HF in APD prolongation and increased STV, especially at slow heart rates. I_{NaL} increase and its consequences may be exacerbated on sympathetic activation. Our results agree with previous studies showing beneficial effects of I_{NaL} inhibition in HF and point to I_{NaL} as a therapeutic target to reduce the risk of arrhythmias in HF.[18,24] However, it should be considered that selective I_{NaL} inhibition decreased APD, albeit more modestly, in control. On the contrary, hyporesponsiveness of I_{CaL} to βAR stimulation limits Ca^{2+} entry, and that can aggravate the contractile deficit in HF. Our data demonstrate the importance of utilizing physiological recording conditions when measuring ionic currents, especially in cardiac pathologies associated with altered $[Ca^{2+}]_i$ handing and CaMKII activity, to improve our understanding of electrophysiological remodeling and mechanistic bases of arrhythmogenesis in HF.

ARTICLE INFORMATION

Received November 19, 2018; accepted February 13, 2019.

The Data Supplement is available at https://www.ahajournals.org/doi/suppl/10.1161/CIRCEP.118.007061.

Correspondence

Donald M. Bers, PhD, Department of Pharmacology, University of California, Davis, 451 Health Sciences Dr, Davis, CA 95616. Email dmbers@ucdavis.edu

Affiliations

Department of Pharmacology (B.H., S.M., C.L., K.S.G., J.B., L.T.I., Y.C.-I., T.B., E.G., D.M.B.), Department of Biomedical Engineering (Y.C.-I.), and Department of Internal Medicine/Cardiology (Y.C.-I.), University of California, Davis. Department of Clinical Research, Gilead Sciences, Inc, Foster City, CA (L.B.). Department of Physiology, University of Debrecen, Hungary (T.B.).

Current address for Dr Belardinelli: InCarda Therapeutics, Inc, Newark, CA.

Acknowledgments

We thank Dr William T. Ferrier and Linda Talken for performing the surgical procedures and Lynette M. Mendoza for performing echocardiography. We also thank Logan R.J. Bailey, Johanna M. Borst, Austen J. Lucena, Maura Ferrero, Matthew L. Stein, Ian P. Palmer, and Maximilien Bergman for their help in animal care and cell isolation.

Sources of Funding

This work was supported by grants from the National Institutes of Health P01-HL080101 and R01-HL030077 (Dr Bers), R01-HL142282 (Drs Bers and Bossuyt), OT2-OD023848, OT2-OD026580 and R01-HL131517, R01-HL141214 (Dr Grandi), R01-HL090880 (Drs Izu and Chen-Izu), R01-HL123526 (Dr Chen-Izu), and K99-HL138160 (Dr Morotti); the American Heart Association 14GRNT20510041 (Dr Chen-Izu) and 15SDG24910015 (Dr Grandi); the Hungarian Scientific Research Fund OTKA101196 (Dr Bányász); the Heart Rhythm Society postdoctoral fellowship 16OA9HRS (Dr Morotti); and the UC Davis School of Medicine Dean's Fellow Award (Dr Grandi).

Disclosures

Dr Belardinelli is a former employee of Gilead Sciences, Inc, which is the patent holder of GS-967. The other authors report no conflicts.

REFERENCES

1. Volders PG, Vos MA, Szabo B, Sipido KR, de Groot SH, Gorgels AP, Wellens HJ, Lazzara R. Progress in the understanding of cardiac early afterdepolarizations and torsades de pointes: time to revise current concepts. *Cardiovasc Res*. 2000;46:376–392.
2. Weiss JN, Garfinkel A, Karagueuzian HS, Chen PS, Qu Z. Early afterdepolarizations and cardiac arrhythmias. *Heart Rhythm*. 2010;7:1891–1899. doi: 10.1016/j.hrthm.2010.09.017
3. Verkerk AO, Veldkamp MW, Baartscheer A, Schumacher CA, Klöpping C, van Ginneken AC, Ravesloot JH. Ionic mechanism of delayed afterdepolarizations in ventricular cells isolated from human end-stage failing hearts. *Circulation*. 2001;104:2728–2733.

4. Pogwizd SM, Schlotthauer K, Li L, Yuan W, Bers DM. Arrhythmogenesis and contractile dysfunction in heart failure: roles of sodium-calcium exchange, inward rectifier potassium current, and residual beta-adrenergic responsiveness. *Circ Res*. 2001;88:1159–1167.
5. Kääb S, Nuss HB, Chiamvimonvat N, O'Rourke B, Pak PH, Kass DA, Marban E, Tomaselli GF. Ionic mechanism of action potential prolongation in ventricular myocytes from dogs with pacing-induced heart failure. *Circ Res*. 1996;78:262–273.
6. Tomaselli GF, Beuckelmann DJ, Calkins HG, Berger RD, Kessler PD, Lawrence JH, Kass D, Feldman AM, Marban E. Sudden cardiac death in heart failure. The role of abnormal repolarization. *Circulation*. 1994;90:2534–2539.
7. Maltsev VA, Silverman N, Sabbah HN, Undrovinas AI. Chronic heart failure slows late sodium current in human and canine ventricular myocytes: implications for repolarization variability. *Eur J Heart Fail*. 2007;9:219–227. doi: 10.1016/j.ejheart.2006.08.007
8. Piccirillo G, Magrì D, Matera S, Magnanti M, Torrini A, Pasquazzi E, Schifano E, Velitti S, Marigliano V, Quaglione R, Barillà F. QT variability strongly predicts sudden cardiac death in asymptomatic subjects with mild or moderate left ventricular systolic dysfunction: a prospective study. *Eur Heart J*. 2007;28:1344–1350. doi: 10.1093/eurheartj/ehl367
9. Pogwizd SM, Qi M, Yuan W, Samarel AM, Bers DM. Upregulation of Na(+)/Ca(2+) exchanger expression and function in an arrhythmogenic rabbit model of heart failure. *Circ Res*. 1999;85:1009–1019.
10. Weber CR, Piacentino V 3rd, Houser SR, Bers DM. Dynamic regulation of sodium/calcium exchange function in human heart failure. *Circulation*. 2003;108:2224–2229. doi: 10.1161/01.CIR.0000095274.72486.94
11. Maltsev VA, Sabbah HN, Higgins RS, Silverman N, Lesch M, Undrovinas AI. Novel, ultraslow inactivating sodium current in human ventricular cardiomyocytes. *Circulation*. 1998;98:2545–2552.
12. Valdivia CR, Chu WW, Pu J, Foell JD, Haworth RA, Wolff MR, Kamp TJ, Makielski JC. Increased late sodium current in myocytes from a canine heart failure model and from failing human heart. *J Mol Cell Cardiol*. 2005;38:475–483. doi: 10.1016/j.yjmcc.2004.12.012
13. Beuckelmann DJ, Näbauer M, Erdmann E. Alterations of K+ currents in isolated human ventricular myocytes from patients with terminal heart failure. *Circ Res*. 1993;73:379–385.
14. Hegyi B, Bossuyt J, Ginsburg KS, Mendoza LM, Talken L, Ferrier WT, Pogwizd SM, Izu LT, Chen-Izu Y, Bers DM. Altered repolarization reserve in failing rabbit ventricular myocytes: calcium and β-adrenergic effects on delayed- and inward-rectifier potassium currents. *Circ Arrhythm Electrophysiol*. 2018;11:e005852. doi: 10.1161/CIRCEP.117.005852
15. Kääb S, Dixon J, Duc J, Ashen D, Näbauer M, Beuckelmann DJ, Steinbeck G, McKinnon D, Tomaselli GF. Molecular basis of transient outward potassium current downregulation in human heart failure: a decrease in Kv4.3 mRNA correlates with a reduction in current density. *Circulation*. 1998;98:1383–1393.
16. Rivaud MR, Agullo-Pascual E, Lin X, Leo-Macias A, Zhang M, Rothenberg E, Bezzina CR, Delmar M, Remme CA. Sodium channel remodeling in subcellular microdomains of murine failing cardiomyocytes. *J Am Heart Assoc*. 2017;6:e007622.
17. Wagner S, Dybkova N, Rasenack EC, Jacobshagen C, Fabritz L, Kirchhof P, Maier SK, Zhang T, Hasenfuss G, Brown JH, Bers DM, Maier LS. Ca2+/calmodulin-dependent protein kinase II regulates cardiac Na+ channels. *J Clin Invest*. 2006;116:3127–3138. doi: 10.1172/JCI26620
18. Toischer K, Hartmann N, Wagner S, Fischer TH, Herting J, Danner BC, Sag CM, Hund TJ, Mohler PJ, Belardinelli L, Hasenfuss G, Maier LS, Sossalla S. Role of late sodium current as a potential arrhythmogenic mechanism in the progression of pressure-induced heart disease. *J Mol Cell Cardiol*. 2013;61:111–122. doi: 10.1016/j.yjmcc.2013.03.021
19. Koval OM, Snyder JS, Wolf RM, Pavlovicz RE, Glynn P, Curran J, Leymaster ND, Dun W, Wright PJ, Cardona N, Qian L, Mitchell CC, Boyden PA, Binkley PF, Li C, Anderson ME, Mohler PJ, Hund TJ. Ca2+/calmodulin-dependent protein kinase II-based regulation of voltage-gated Na+ channel in cardiac disease. *Circulation*. 2012;126:2084–2094. doi: 10.1161/CIRCULATIONAHA.112.105320
20. Horvath B, Banyasz T, Jian Z, Hegyi B, Kistamas K, Nanasi PP, Izu LT, Chen-Izu Y. Dynamics of the late Na(+) current during cardiac action potential and its contribution to afterdepolarizations. *J Mol Cell Cardiol*. 2013;64:59–68. doi: 10.1016/j.yjmcc.2013.08.010
21. Hegyi B, Bányász T, Izu LT, Belardinelli L, Bers DM, Chen-Izu Y. β-adrenergic regulation of late Na+ current during cardiac action potential is mediated by both PKA and CaMKII. *J Mol Cell Cardiol*. 2018;123:168–179. doi: 10.1016/j.yjmcc.2018.09.006
22. Matsuda JJ, Lee H, Shibata EF. Enhancement of rabbit cardiac sodium channels by beta-adrenergic stimulation. *Circ Res*. 1992;70:199–207.
23. Belardinelli L, Giles WR, Rajamani S, Karagueuzian HS, Shryock JC. Cardiac late Na^+ current: proarrhythmic effects, roles in long QT syndromes, and pathological relationship to CaMKII and oxidative stress. *Heart Rhythm*. 2015;12:440–448. doi: 10.1016/j.hrthm.2014.11.009
24. Sag CM, Mallwitz A, Wagner S, Hartmann N, Schotola H, Fischer TH, Ungeheuer N, Herting J, Shah AM, Maier LS, Sossalla S, Unsöld B. Enhanced late INa induces proarrhythmogenic SR Ca leak in a CaMKII-dependent manner. *J Mol Cell Cardiol*. 2014;76:94–105. doi: 10.1016/j.yjmcc.2014.08.016
25. Tomaselli GF, Marbán E. Electrophysiological remodeling in hypertrophy and heart failure. *Cardiovasc Res*. 1999;42:270–283.
26. Nattel S, Maguy A, Le Bouter S, Yeh YH. Arrhythmogenic ion-channel remodeling in the heart: heart failure, myocardial infarction, and atrial fibrillation. *Physiol Rev*. 2007;87:425–456. doi: 10.1152/physrev.00014.2006
27. Anderson ME, Braun AP, Schulman H, Premack BA. Multifunctional Ca2+/calmodulin-dependent protein kinase mediates Ca(2+)-induced enhancement of the L-type Ca2+ current in rabbit ventricular myocytes. *Circ Res*. 1994;75:854–861.
28. Hudmon A, Schulman H, Kim J, Maltez JM, Tsien RW, Pitt GS. CaMKII tethers to L-type Ca2+ channels, establishing a local and dedicated integrator of Ca2+ signals for facilitation. *J Cell Biol*. 2005;171:537–547. doi: 10.1083/jcb.200505155
29. Bers DM, Morotti S. Ca(2+) current facilitation is CaMKII-dependent and has arrhythmogenic consequences. *Front Pharmacol*. 2014;5:144. doi: 10.3389/fphar.2014.00144
30. Hoeker GS, Hanafy MA, Oster RA, Bers DM, Pogwizd SM. Reduced arrhythmia inducibility with calcium/calmodulin-dependent protein kinase II inhibition in heart failure rabbits. *J Cardiovasc Pharmacol*. 2016;67:260–265. doi: 10.1097/FJC.0000000000000343
31. Banyasz T, Horvath B, Jian Z, Izu LT, Chen-Izu Y. Profile of L-type Ca(2+) current and Na(+)/Ca(2+) exchange current during cardiac action potential in ventricular myocytes. *Heart Rhythm*. 2012;9:134–142. doi: 10.1016/j.hrthm.2011.08.029
32. Horváth B, Váczi K, Hegyi B, Gönczi M, Dienes B, Kistamás K, Bányász T, Magyar J, Baczkó I, Varró A, Seprényi G, Csernoch L, Nánási PP, Szentandrássy N. Sarcolemmal Ca(2+)-entry through L-type Ca(2+) channels controls the profile of Ca(2+)-activated Cl(-) current in canine ventricular myocytes. *J Mol Cell Cardiol*. 2016;97:125–139. doi: 10.1016/j.yjmcc.2016.05.006
33. Szentandrássy N, Kistamás K, Hegyi B, Horváth B, Ruzsnavszky F, Váczi K, Magyar J, Bányász T, Varró A, Nánási PP. Contribution of ion currents to beat-to-beat variability of action potential duration in canine ventricular myocytes. *Pflugers Arch*. 2015;467:1431–1443. doi: 10.1007/s00424-014-1581-4
34. Chen-Izu Y, Izu LT, Hegyi B, Bányász T. Recording of ionic currents under physiological conditions: action potential-clamp and 'onion-peeling' techniques. In: Jue T, ed. *Modern Tools of Biophysics*. New York, NY: Springer New York; 2017:31–48.
35. Banyasz T, Horvath B, Jian Z, Izu LT, Chen-Izu Y. Sequential dissection of multiple ionic currents in single cardiac myocytes under action potential-clamp. *J Mol Cell Cardiol*. 2011;50:578–581. doi: 10.1016/j.yjmcc.2010.12.020
36. Bartos DC, Morotti S, Ginsburg KS, Grandi E, Bers DM. Quantitative analysis of the Ca2+ -dependent regulation of delayed rectifier K+ current IKs in rabbit ventricular myocytes. *J Physiol*. 2017;595:2253–2268. doi: 10.1113/JP273676
37. Shannon TR, Wang F, Puglisi J, Weber C, Bers DM. A mathematical treatment of integrated Ca dynamics within the ventricular myocyte. *Biophys J*. 2004;87:3351–3371. doi: 10.1529/biophysj.104.047449
38. Soltis AR, Saucerman JJ. Synergy between CaMKII substrates and β-adrenergic signaling in regulation of cardiac myocyte Ca(2+) handling. *Biophys J*. 2010;99:2038–2047. doi: 10.1016/j.bpj.2010.08.016
39. Negroni JA, Morotti S, Lascano EC, Gomes AV, Grandi E, Puglisi JL, Bers DM. β-adrenergic effects on cardiac myofilaments and contraction in an integrated rabbit ventricular myocyte model. *J Mol Cell Cardiol*. 2015;81:162–175. doi: 10.1016/j.yjmcc.2015.02.014
40. Shannon TR, Wang F, Bers DM. Regulation of cardiac sarcoplasmic reticulum Ca release by luminal [Ca] and altered gating assessed with a mathematical model. *Biophys J*. 2005;89:4096–4110. doi: 10.1529/biophysj.105.068734
41. Despa S, Islam MA, Weber CR, Pogwizd SM, Bers DM. Intracellular Na(+) concentration is elevated in heart failure but Na/K pump function is unchanged. *Circulation*. 2002;105:2543–2548.

42. Huang B, El-Sherif T, Gidh-Jain M, Qin D, El-Sherif N. Alterations of sodium channel kinetics and gene expression in the postinfarction remodeled myocardium. *J Cardiovasc Electrophysiol*. 2001;12:218–225.
43. Mishra S, Reznikov V, Maltsev VA, Undrovinas NA, Sabbah HN, Undrovinas A. Contribution of sodium channel neuronal isoform Nav1.1 to late sodium current in ventricular myocytes from failing hearts. *J Physiol*. 2015;593:1409–1427. doi: 10.1113/jphysiol.2014.278259
44. Clancy CE, Chen-Izu Y, Bers DM, Belardinelli L, Boyden PA, Csernoch L, Despa S, Fermini B, Hool LC, Izu L, Kass RS, Lederer WJ, Louch WE, Maack C, Matiazzi A, Qu Z, Rajamani S, Rippinger CM, Sejersted OM, O'Rourke B, Weiss JN, Varró A, Zaza A. Deranged sodium to sudden death. *J Physiol*. 2015;593:1331–1345. doi: 10.1113/jphysiol.2014.281204
45. Wagner S, Ruff HM, Weber SL, Bellmann S, Sowa T, Schulte T, Anderson ME, Grandi E, Bers DM, Backs J, Belardinelli L, Maier LS. Reactive oxygen species-activated Ca/calmodulin kinase IIδ is required for late I(Na) augmentation leading to cellular Na and Ca overload. *Circ Res*. 2011;108:555–565. doi: 10.1161/CIRCRESAHA.110.221911
46. Morotti S, Edwards AG, McCulloch AD, Bers DM, Grandi E. A novel computational model of mouse myocyte electrophysiology to assess the synergy between Na+ loading and CaMKII. *J Physiol*. 2014;592:1181–1197. doi: 10.1113/jphysiol.2013.266676
47. Schröder F, Handrock R, Beuckelmann DJ, Hirt S, Hullin R, Priebe L, Schwinger RH, Weil J, Herzig S. Increased availability and open probability of single L-type calcium channels from failing compared with nonfailing human ventricle. *Circulation*. 1998;98:969–976.
48. Findlay I. Voltage- and cation-dependent inactivation of L-type Ca2+ channel currents in guinea-pig ventricular myocytes. *J Physiol*. 2002;541(pt 3):731–740.
49. Weber CR, Piacentino V 3rd, Ginsburg KS, Houser SR, Bers DM. Na(+)-Ca(2+) exchange current and submembrane [Ca(2+)] during the cardiac action potential. *Circ Res*. 2002;90:182–189.
50. Grandi E, Pasqualini FS, Bers DM. A novel computational model of the human ventricular action potential and Ca transient. *J Mol Cell Cardiol*. 2010;48:112–121. doi: 10.1016/j.yjmcc.2009.09.019
51. Hegyi B, Bossuyt J, Griffiths LG, Shimkunas R, Coulibaly Z, Jian Z, Grimsrud KN, Sondergaard CS, Ginsburg KS, Chiamvimonvat N, Belardinelli L, Varró A, Papp JG, Pollesello P, Levijoki J, Izu LT, Boyd WD, Bányász T, Bers DM, Chen-Izu Y. Complex electrophysiological remodeling in postinfarction ischemic heart failure. *Proc Natl Acad Sci USA*. 2018;115:E3036–E3044. doi: 10.1073/pnas.1718211115
52. Ai X, Curran JW, Shannon TR, Bers DM, Pogwizd SM. Ca2+/calmodulin-dependent protein kinase modulates cardiac ryanodine receptor phosphorylation and sarcoplasmic reticulum Ca2+ leak in heart failure. *Circ Res*. 2005;97:1314–1322. doi: 10.1161/01.RES.0000194329.41863.89
53. Curran J, Brown KH, Santiago DJ, Pogwizd S, Bers DM, Shannon TR. Spontaneous Ca waves in ventricular myocytes from failing hearts depend on Ca(2+)-calmodulin-dependent protein kinase II. *J Mol Cell Cardiol*. 2010;49:25–32. doi: 10.1016/j.yjmcc.2010.03.013
54. Vermeulen JT, McGuire MA, Opthof T, Coronel R, de Bakker JM, Klöpping C, Janse MJ. Triggered activity and automaticity in ventricular trabeculae of failing human and rabbit hearts. *Cardiovasc Res*. 1994;28:1547–1554.
55. Davey PP, Barlow C, Hart G. Prolongation of the QT interval in heart failure occurs at low but not at high heart rates. *Clin Sci (Lond)*. 2000;98:603–610.
56. Wu L, Ma J, Li H, Wang C, Grandi E, Zhang P, Luo A, Bers DM, Shryock JC, Belardinelli L. Late sodium current contributes to the reverse rate-dependent effect of IKr inhibition on ventricular repolarization. *Circulation*. 2011;123:1713–1720. doi: 10.1161/CIRCULATIONAHA.110.000661
57. Baartscheer A, Schumacher CA, Belterman CN, Coronel R, Fiolet JW. SR calcium handling and calcium after-transients in a rabbit model of heart failure. *Cardiovasc Res*. 2003;58:99–108.
58. Johnson DM, Heijman J, Bode EF, Greensmith DJ, van der Linde H, Abi-Gerges N, Eisner DA, Trafford AW, Volders PG. Diastolic spontaneous calcium release from the sarcoplasmic reticulum increases beat-to-beat variability of repolarization in canine ventricular myocytes after β-adrenergic stimulation. *Circ Res*. 2013;112:246–256. doi: 10.1161/CIRCRESAHA.112.275735
59. Gomez JF, Cardona K, Trenor B. Lessons learned from multi-scale modeling of the failing heart. *J Mol Cell Cardiol*. 2015;89(pt B):146–159. doi: 10.1016/j.yjmcc.2015.10.016
60. Hegyi B, Bers DM, Bossuyt J. CaMKII signaling in heart diseases: emerging role in diabetic cardiomyopathy. *J Mol Cell Cardiol*. 2019;127:246–259. doi: 10.1016/j.yjmcc.2019.01.001
61. Peterson BZ, DeMaria CD, Adelman JP, Yue DT. Calmodulin is the Ca2+ sensor for Ca2+ -dependent inactivation of L-type calcium channels. *Neuron*. 1999;22:549–558.
62. Grandi E, Morotti S, Ginsburg KS, Severi S, Bers DM. Interplay of voltage and Ca-dependent inactivation of L-type Ca current. *Prog Biophys Mol Biol*. 2010;103:44–50. doi: 10.1016/j.pbiomolbio.2010.02.001
63. Sarhan MF, Tung CC, Van Petegem F, Ahern CA. Crystallographic basis for calcium regulation of sodium channels. *Proc Natl Acad Sci USA*. 2012;109:3558–3563. doi: 10.1073/pnas.1114748109
64. Maltsev VA, Reznikov V, Undrovinas NA, Sabbah HN, Undrovinas A. Modulation of late sodium current by Ca2+, calmodulin, and CaMKII in normal and failing dog cardiomyocytes: similarities and differences. *Am J Physiol Heart Circ Physiol*. 2008;294:H1597–H1608. doi: 10.1152/ajpheart.00484.2007
65. Chen-Izu Y, Shaw RM, Pitt GS, Yarov-Yarovoy V, Sack JT, Abriel H, Aldrich RW, Belardinelli L, Cannell MB, Catterall WA, Chazin WJ, Chiamvimonvat N, Deschenes I, Grandi E, Hund TJ, Izu LT, Maier LS, Maltsev VA, Marionneau C, Mohler PJ, Rajamani S, Rasmusson RL, Sobie EA, Clancy CE, Bers DM. Na+ channel function, regulation, structure, trafficking and sequestration. *J Physiol*. 2015;593:1347–1360. doi: 10.1113/jphysiol.2014.281428
66. Hullin R, Matthes J, von Vietinghoff S, Bodi I, Rubio M, D'Souza K, Friedrich Khan I, Rottländer D, Hoppe UC, Mohacsi P, Schmitteckert E, Gilsbach R, Bünemann M, Hein L, Schwartz A, Herzig S. Increased expression of the auxiliary beta(2)-subunit of ventricular L-type Ca(2)+ channels leads to single-channel activity characteristic of heart failure. *PLoS One*. 2007;2:e292. doi: 10.1371/journal.pone.0000292
67. Colecraft HM, Alseikhan B, Takahashi SX, Chaudhuri D, Mittman S, Yegnasubramanian V, Alvania RS, Johns DC, Marbán E, Yue DT. Novel functional properties of Ca(2+) channel beta subunits revealed by their expression in adult rat heart cells. *J Physiol*. 2002;541(pt 2):435–452.
68. Miriyala J, Nguyen T, Yue DT, Colecraft HM. Role of CaVbeta subunits, and lack of functional reserve, in protein kinase A modulation of cardiac CaV1.2 channels. *Circ Res*. 2008;102:e54–e64. doi: 10.1161/CIRCRESAHA.108.171736
69. Beetz N, Hein L, Meszaros J, Gilsbach R, Barreto F, Meissner M, Hoppe UC, Schwartz A, Herzig S, Matthes J. Transgenic simulation of human heart failure-like L-type Ca2+-channels: implications for fibrosis and heart rate in mice. *Cardiovasc Res*. 2009;84:396–406. doi: 10.1093/cvr/cvp251
70. Desantiago J, Ai X, Islam M, Acuna G, Ziolo MT, Bers DM, Pogwizd SM. Arrhythmogenic effects of beta2-adrenergic stimulation in the failing heart are attributable to enhanced sarcoplasmic reticulum Ca load. *Circ Res*. 2008;102:1389–1397. doi: 10.1161/CIRCRESAHA.107.169011
71. Barbagallo F, Xu B, Reddy GR, West T, Wang Q, Fu Q, Li M, Shi Q, Ginsburg KS, Ferrier W, Isidori AM, Naro F, Patel HH, Bossuyt J, Bers D, Xiang YK. Genetically encoded biosensors reveal PKA hyperphosphorylation on the myofilaments in rabbit heart failure. *Circ Res*. 2016;119:931–943. doi: 10.1161/CIRCRESAHA.116.308964
72. Katchman A, Yang L, Zakharov SI, Kushner J, Abrams J, Chen BX, Liu G, Pitt GS, Colecraft HM, Marx SO. Proteolytic cleavage and PKA phosphorylation of α1C subunit are not required for adrenergic regulation of CaV1.2 in the heart. *Proc Natl Acad Sci USA*. 2017;114:9194–9199. doi: 10.1073/pnas.1706054114
73. Herren AW, Weber DM, Rigor RR, Margulies KB, Phinney BS, Bers DM. CaMKII phosphorylation of Na(V)1.5: novel *in vitro* sites identified by mass spectrometry and reduced S516 phosphorylation in human heart failure. *J Proteome Res*. 2015;14:2298–2311. doi: 10.1021/acs.jproteome.5b00107

SUPPLEMENTAL MATERIAL

Supplemental Table. Inactivation parameters of L-type Ca^{2+} current (I_{CaL}) in control and heart failure (HF).

	Control		HF	
I_{CaL} parameter	Experiment	Model	Experiment	Model
Peak (A/F)	12.0±0.9	12.7	11.4±1.1	13.1
τ fast (ms)	16.4±0.4	28.5	19.6±0.6	28.4
Amplitude fast (%)	78.2±1.1	76.8	80.7±1.9	76.6
τ slow (ms)	86.9±4.2	119.7	106.8±6.5	114.6
Amplitude slow (%)	21.8±1.1	23.2	19.3±1.9	23.4

Inactivation parameters of I_{CaL} were assessed at 0 mV by biexponential fitting of the current decay. I_{CaL} parameters measured in isolated cardiomyoyctes are expressed as mean±SEM. n=6 cells from 3 animals for both control and HF. See Methods for details of I_{CaL} modeling.

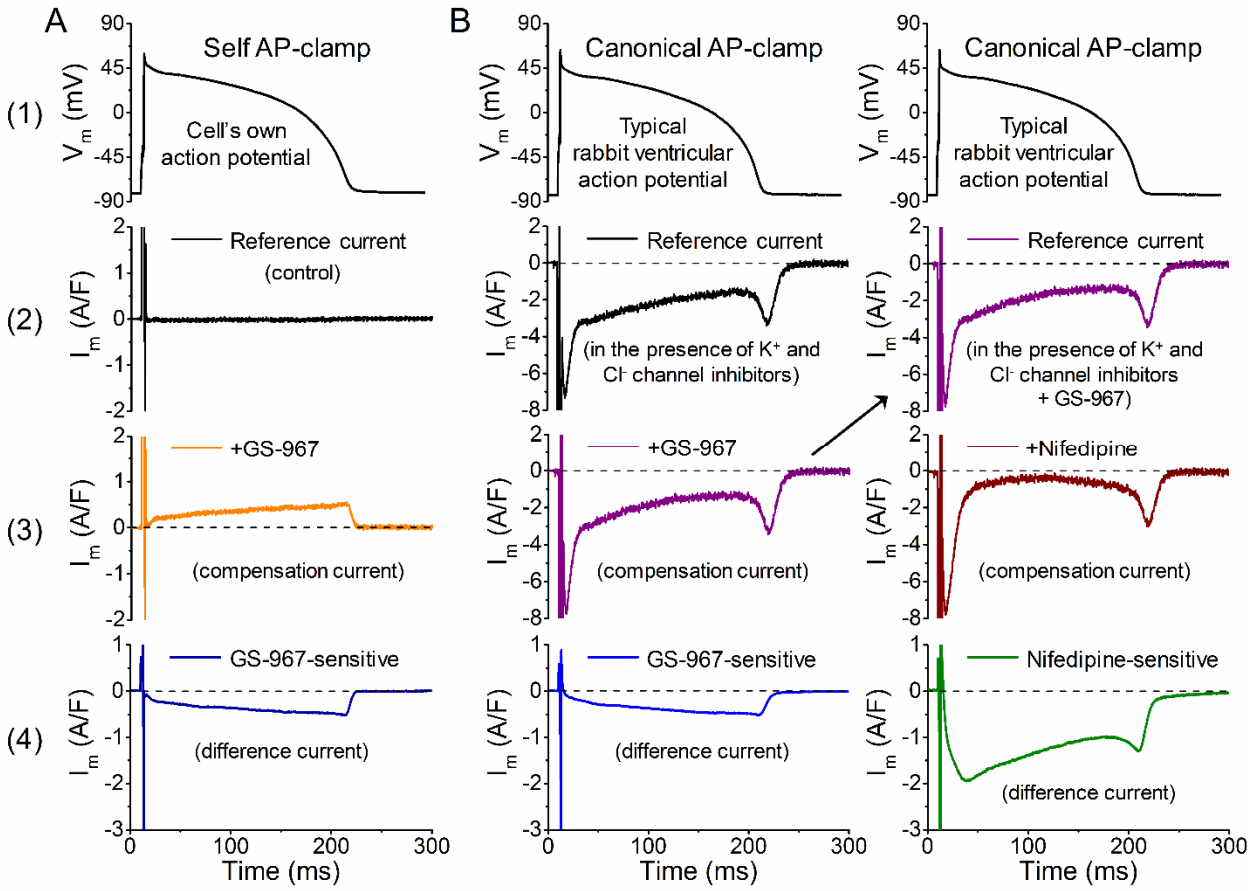

Supplemental Figure I. Action potential (AP)-clamp technique.
Representative traces show the basic steps of self AP-clamp (**A**) and canonical AP-clamp (**B**) experiments. First, using an AP as voltage command (1) a reference current is recorded (2). Next, when the drug is applied and reached its steady-state effect, a compensation current is recorded specific to the drug action (3). The drug-sensitive current is obtained as the difference current (i.e. subtracting the compensation current from the reference current) (4). In self AP-clamp (**A**) the cell's own steady-state AP is applied and the reference current should be zero. When the cell is pretreated with different ion channel inhibitors and a prerecorded, typical rabbit AP (canonical AP-clamp, **B**) is applied, the reference current is no longer flat. However, the reference current still must reach a steady-state indicating stable seal conditions. Under AP-clamp, all ionic currents were recorded as difference currents after their specific blocker had reached steady-state effect (3-min perfusion). 60 consecutive traces were recorded (to evaluate the stability of the reference and compensation currents) and averaged in each case before and 3-min after drug application. 1 µmol/L GS-967 and 10 µmol/L nifedipine were used to measure late Na^+ current (I_{NaL}) and L-type Ca^{2+} current (I_{CaL}), respectively.

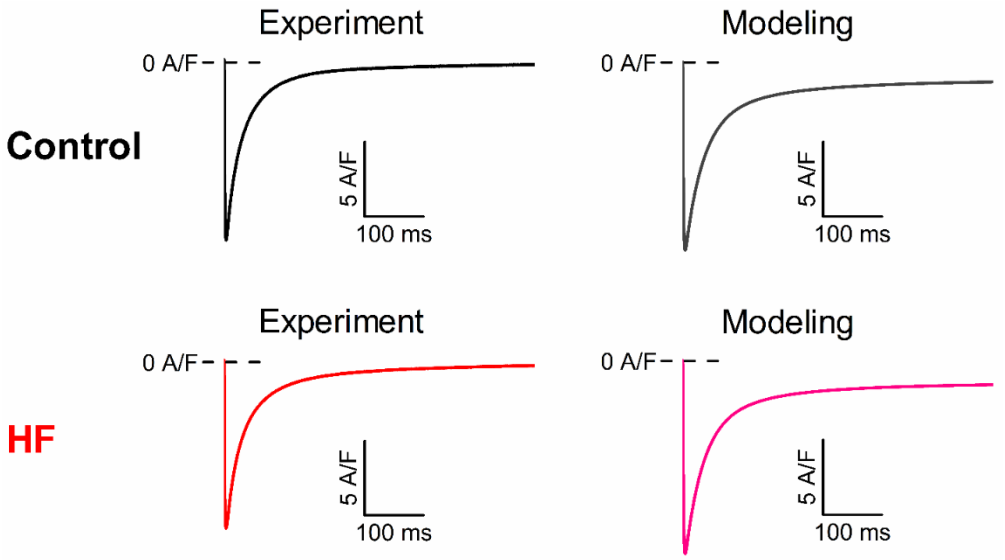

Supplemental Figure II. Modeling of L-type Ca^{2+} current (I_{CaL}) in control and heart failure (HF). Representative I_{CaL} traces measured at 0 mV with square pulse voltage protocol in isolated cardiomyocytes (left) and in silico (right) in control (black/grey) and in HF (red/pink). I_{CaL} was measured in the presence of 5 mmol/L EGTA ($[Ca^{2+}]_i$=100 nmol/L) in the pipette. Inactivation parameters of I_{CaL} are shown in Figure 4E and Supplemental Table.

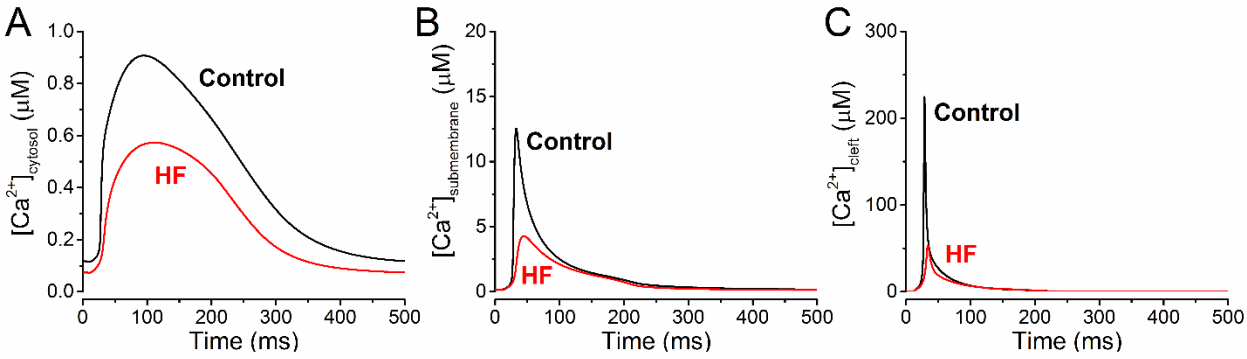

Supplemental Figure III. Physiological Ca^{2+} transient in control and heart failure (HF).
Physiological Ca^{2+} transients have been obtained with our updated rabbit ventricular myocyte model that integrates detailed descriptions of electrophysiology, Ca^{2+} and Na^{+} handling, PKA and CaMKII signaling, and myofilament contraction. Simulated Ca^{2+} transients under AP-clamp at 2 Hz pacing in control and HF in the cytosol (**A**), in the submembrane compartment (**B**), and in the dyadic cleft (**C**).

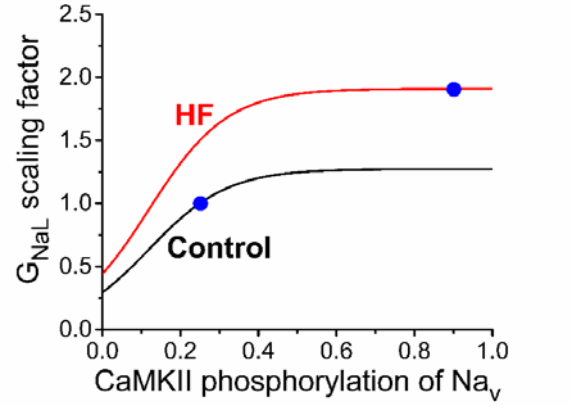

Supplemental Figure IV. Modeling the CaMKII-dependent modulation of late Na^+ current (I_{NaL}). Relationship between the CaMKII-dependent phosphorylation of voltage-gated Na^+ channel (Na_V) and the conductance of late Na^+ current (G_{NaL}). The scaling factor that multiplies the basal G_{NaL} value of 0.0527 is shown (control in black, HF in red). Basal G_{NaL} is increased by 50% in HF. By design, the scaling factor is 1 for control with physiologic Ca^{2+} transient at 2 Hz pacing. CaMKII-dependent Na_V phosphorylation is ≈25% in control and ≈90% in HF with physiologic Ca^{2+} transient (blue circles).